
FZOO: Fast Zeroth-Order Optimizer for Fine-Tuning Large Language Models towards Adam-Scale Speed

Sizhe Dang*
Xi'an Jiaotong University

Yangyang Guo*
Xi'an Jiaotong University

Yanjun Zhao*
Xi'an Jiaotong University

Haishan Ye*†
Xi'an Jiaotong University
SGIT AI Lab

Xiaodong Zheng
Xi'an Jiaotong University

Guang Dai
SGIT AI Lab

Ivor Tsang
A*STAR

{darknight1118, no.314016, yanjun.zhao, zxd_xjtu}@stu.xjtu.edu.cn
yehaishan@xjtu.edu.cn, guang.dai@gmail.com, ivor_tsang@cfar.a-star.edu.sg

Abstract

Fine-tuning large language models (LLMs) often faces GPU memory bottlenecks: the backward pass of first-order optimizers like Adam increases memory usage to more than 10 times the inference level (e.g., 633 GB for OPT-30B). Zeroth-order (ZO) optimizers avoid this cost by estimating gradients only from forward passes, yet existing methods like MeZO usually need tens of times more steps to converge. Can this trade-off between speed and memory in ZO be fundamentally improved? Normalized-SGD, for instance, demonstrates strong empirical performance with greater memory efficiency than Adam. In light of this, we introduce **FZOO**, a Fast Zeroth-Order Optimizer towards Adam-Scale Speed. On the one hand, FZOO reduces the total forward passes needed for convergence by employing batched one-sided estimates that adapt step-sizes based on the standard deviation of batch losses. On the other hand, it accelerates per-batch computation through the use of Rademacher random vector (± 1) perturbations coupled with CUDA's parallel processing capabilities. Extensive experiments on diverse models (including RoBERTa-large, the OPT family (350M-66B), Phi-2, and Llama3) across 11 varied downstream tasks validate FZOO's effectiveness. On average, FZOO outperforms MeZO by +3% in accuracy while requiring $3\times$ fewer forward passes. Notably, for the RoBERTa-large model, FZOO achieves average improvements of +5.6% in accuracy and $18\times$ reduction in forward passes compared to MeZO, achieving convergence speeds comparable to Adam. We also provide theoretical analysis proving FZOO's formal equivalence to a normalized-SGD update rule and establishing its convergence guarantees. Beyond full-parameter tuning, FZOO plugs smoothly into PEFT techniques, unlocking even larger memory savings. Taken together, our results make single-GPU, high-speed, full-parameter fine-tuning realistic today and point toward future work on memory-efficient pre-training. **Project Homepage:** https://dkmiyan.github.io/FZOO_hp

1 Introduction

Large language models (LLMs) have become the workhorse of natural-language and multi-modal applications [12, 16, 30], yet they often require additional fine-tuning to excel on downstream tasks. Current practice relies on first-order optimizers such as Adam [20], whose backward pass stores all

*Equal contribution.

†Corresponding author.

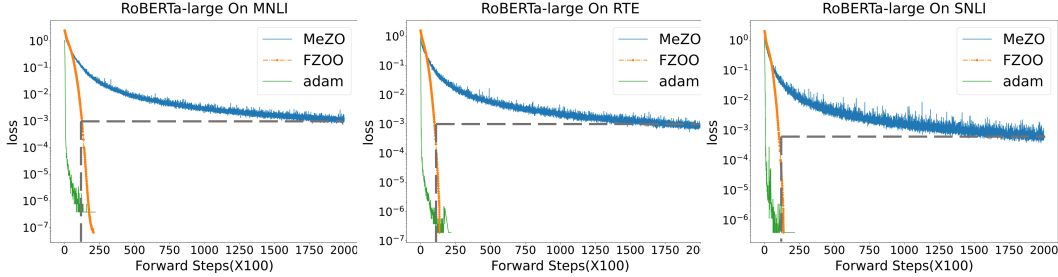


Figure 1: Performance of MeZO, Adam and FZOO on different tasks when fine-tuning RoBERTa-large model. For the sake of uniform comparison, we convert Adam’s backward pass into 3 forward passes. FZOO can achieve $18\times$ speedup compared with MeZO, nearly $20\times$ that of Adam.

activations and gradients, linearly multiplying the memory cost—fine-tuning an OPT-30B model then consumes **633 GB** of GPU memory, more than **10 \times** its inference memory cost. This creates the *memory wall* that now limits model training in resource-constrained scenarios.

Two main strategies have been explored to overcome this wall. *Parameter-efficient tuning* (PEFT) [18, 22, 11, 51, 31] (e.g., LoRA [18]) updates only a small subset of weights and thus lowers memory cost, but it still requires the backward pass and can lag full-parameter tuning (FT) on some difficult tasks. The other approach turns to *zeroth-order* (ZO) optimization [28, 52]: methods such as MeZO [28] use multiple forward passes to replace the backward pass when estimating gradients. This brings the memory overhead of fine-tuning down to the inference level, but this benefit comes with a significant trade-off in speed, as convergence is often about $20\times$ slower than Adam on RoBERTa-large (Figure 1). **Does the use of zeroth-order methods always lead to a trade-off between speed and memory?**

We believe the answer is **no**. This is because ZO performance can be substantially enhanced in three key areas: (i) **Adaptive Step-Sizes**. While Adam uses costly momentum for adaptive steps, normalized-SGD adapts efficiently via gradient normalization without this overhead. Existing ZO methods, however, use inefficient fixed step-sizes for LLM fine-tuning. (ii) **Efficient Query Processing**. Furthermore, each ZO gradient estimate typically requires multiple forward queries. The overall speed of this multi-query process, however, is often hindered by both the computational expense of conventional perturbation sampling (e.g., Gaussian noise) and execution strategies that underutilize parallelism across these queries. (iii) **Engineering Optimization**. Theoretically, one Adam step is twice as fast as a MeZO step (Adam’s backward pass takes roughly three times longer than a forward pass [1], making Adam equivalent to four forward passes versus MeZO’s two). Yet, due to insufficient forward-pass optimizations, MeZO’s actual per-step execution often exceeds Adam’s. Taken together, these observations suggest that a well-engineered ZO optimizer could achieve **Adam-level convergence speed while retaining inference-level memory cost**.

To harness these opportunities for ZO enhancement, we introduce **FZOO**, a **Fast Zeroth-Order Optimizer**. FZOO achieves its significant speed-up through two primary strategies: First, it reduces total convergence passes by employing *batched one-sided estimates*, where the standard deviation of batch losses informs an *adaptive step-size rule*. Second, it accelerates each batch computation using efficient *Rademacher random vector perturbations* (± 1) and *CUDA-optimized parallelism* for the query batches. Specifically, our contributions are:

1. **FZOO**, a novel ZO optimizer that uniquely adapts principles from normalized-SGD to the ZO regime. It is designed to achieve *Adam-scale convergence speed* while operating at an *inference-level memory usage*.
2. We provide rigorous theoretical backing for FZOO, including a formal proof of its equivalence to a normalized-SGD update rule (Section 3.4) and a comprehensive analysis establishing its *convergence guarantees* under standard conditions (Section 3.5).
3. Extensive FT experiments on diverse models (RoBERTa-large, OPT family 350M–66B, Phi-2, and Llama3) across 11 downstream tasks demonstrate FZOO’s superior efficiency (Section 4). On average, FZOO surpasses the MeZO baseline by **+3%** in accuracy with **3 \times** fewer forward passes. Notably, as show in Fig. 1 for the RoBERTa-large model it achieves average improvements of **+5.6%** in accuracy and an **18 \times** reduction in forward passes compared to MeZO, reaching effective convergence speeds *comparable to Adam*.

4. FZOO exhibits strong practical utility, smoothly integrating with PEFT techniques [9, 10] to unlock *even larger memory savings* (Section 4.6). Furthermore, it effectively optimizes both differentiable and non-differentiable objectives during FT (Section 4.3).

2 Related Works

We provide a brief overview of first-order, zeroth-order and batch-based zeroth-order optimizers for large language models; see Appendix A for details.

First-order adaptive methods Standard LLM optimizers include SGD and its refinements [13] like Adam [20], which uses memory-intensive momentum for its adaptive step-sizes. AdamW [27] improves generalization by refining weight decay. Inspiringly, methods like normalized-SGD [2] also adapt steps effectively, often rivaling Adam’s performance but crucially without this significant momentum overhead, offering a key insight for our work. However, all these first-order methods share a fundamental drawback: back-propagation’s requirement to store activations and gradients incurs steep memory costs, severely bottlenecking the fine-tuning of large models.

Zeroth-order optimizers ZO methods sidestep back-prop by estimating gradients with only forward passes. The classic SPSA estimator [33] has powered applications from distributed control [39, 17] to black-box adversarial attacks [6, 4, 24, 44]. MeZO [28] first showed that such forward-only updates can fine-tune LLMs to high accuracy while cutting GPU memory by several times (up to 12×). HiZOO [52] augments MeZO with diagonal Hessian cues to accelerate convergence, but doing so doubles memory and introduces extra hyper-parameters that must be hand-tuned, trading one resource for another. A recent benchmark [49] catalogues many other ZO estimators; nevertheless, none yet approach Adam-Scale speed when constrained to inference-level memory.

Batch-based zeroth-order optimizers A batch-oriented refinement of ZO methods estimates gradients by evaluating a batch of forward step. Recent work like ReLIZO [41] reuses or correlates directions to boost sample efficiency. Augmented Random Search [29] and Evolution Strategies [34, 35] adopt similar population-based updates and are popular in reinforcement learning. However, such approaches generally lack specialized optimizations for accelerating the batched forward process, leading to limited speed when fine-tuning large models.

3 Methods

In the following, we first briefly review the classical zeroth-order gradient estimator employed in MeZO (Section 3.1). We then present the complete workflow of our **FZOO** optimizer (Section 3.2), shown in Figure 2, introduce a parallel perturbation strategy that accelerates computation (Section 3.3), and finally offer a theoretical analysis of the proposed method (Section 3.4, 3.5).

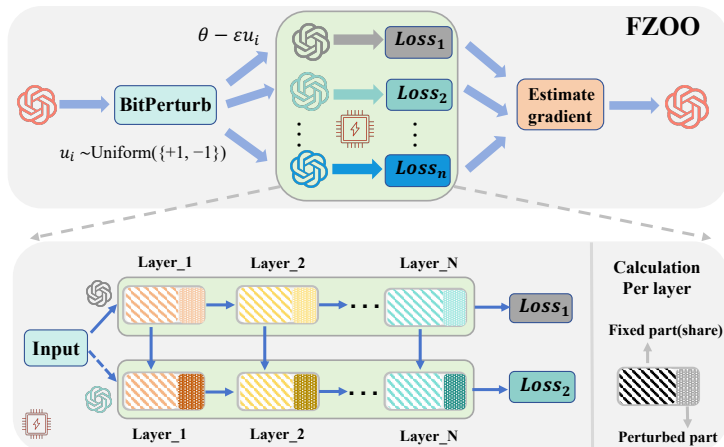


Figure 2: Structure of the of FZOO. The bottom half depicts the toy example of the efficient implementation of batched forward passes.

Algorithm 1 FZOO

Require: parameters $\theta \in \mathbb{R}^d$, loss $L : \mathbb{R}^d \rightarrow \mathbb{R}$, step budget T , perturbation scale ϵ , batch size N , learning rate schedule $\{\eta_t\}$

- 1: **for** $t = 1, \dots, T$ **do**
- 2: $\ell, \theta, seeds \leftarrow \text{BatchPerturbParameters}(\theta, \epsilon, N)$
- 3: $std \leftarrow$ standard deviation of ℓ
- 4: $projected_grad \leftarrow (\ell - \mathcal{L}(\theta; \mathcal{B})) / (N * std)$
- 5: $\text{BatchUpdateParameter}(projected_grad, seeds, \theta, \eta_t)$
- 6: **end for**
- 7: **function** $\text{BATCHPERTURBPARAMETER}(\theta, \epsilon, N)$
- 8: Sample batch $\mathcal{B} \subset \mathcal{D}$; obtain input X and first layer weights $W^{(1)}$
- 9: Initialize random seeds $seeds \leftarrow \{s_1, \dots, s_N\}$
- 10: Generate perturbation vectors $u \in \{\pm 1\}^{N \times d}$ using $seeds$
- 11: Compute unperturbed activations $F^{(1)} \leftarrow W^{(1)} X$
- 12: Compute perturbed activations: $Y_i^{(1)} \leftarrow F^{(1)} + \epsilon(u_i \odot X)$, $i = 1, \dots, N$
- 13: Concatenate activations $Y^{(1)} \leftarrow [Y_1^{(1)}; \dots; Y_N^{(1)}]$
- 14: **for** $j = 2, 3, \dots$ **do**
- 15: $F^{(j)} \leftarrow W^{(j)} Y^{(j-1)}$ ▷ Compute unperturbed activations at layer j
- 16: $P^{(j)} \leftarrow \epsilon(u \odot Y^{(j-1)})$ ▷ Compute perturbations at layer j
- 17: $Y^{(j)} \leftarrow F^{(j)} + P^{(j)}$ ▷ Compute perturbed activations in parallel at layer j
- 18: **end for**
- 19: $\ell \leftarrow \mathcal{L}(Y^{(final)}; \mathcal{B})$ ▷ Compute final losses in parallel
- 20: **return** $\ell, \theta, seeds$
- 21: **end function**
- 22: **function** $\text{BATCHUPDATEPARAMETER}(projected_grad, seeds, \theta, \eta)$
- 23: **for** $idx, s \in \text{enumerate}(seeds)$ **do**
- 24: Reset random number generator with seed s ▷ For sampling u
- 25: **for** $\theta_i \in \theta$ **do**
- 26: $u \sim \text{Uniform}(\{+1, -1\})$
- 27: $\theta_i \leftarrow \theta_i - \eta * projected_grad_{idx} * u$
- 28: **end for**
- 29: **end for**
- 30: **end function**

3.1 Preliminaries

Consider a labelled dataset $\mathcal{D} = \{(x_i, y_i)\}_{i=1}^{|\mathcal{D}|}$ and a mini-batch $\mathcal{B} \subset \mathcal{D}$ of size B . Let $\theta \in \mathbb{R}^d$ denote all trainable parameters of the LLM, and let $L(\theta; \mathcal{B})$ be the empirical loss on \mathcal{B} .

Definition 3.1 (Classical ZO gradient estimation). Given a perturbation radius $\epsilon > 0$ and $z \in \mathbb{R}^d$ sampled as $z \sim \mathcal{N}(0, I_d)$, Classical ZO estimates the gradient on \mathcal{B} via

$$\hat{\nabla} L(\theta; \mathcal{B}) = \frac{L(\theta + \epsilon z; \mathcal{B}) - L(\theta - \epsilon z; \mathcal{B})}{2\epsilon} z \approx z z^\top \nabla L(\theta; \mathcal{B}). \quad (1)$$

Averaging equation 1 over N i.i.d. draws $\{z_i\}_{i=1}^N$ yields the n -ZO estimator $\hat{\nabla}_N L = \frac{1}{N} \sum_{i=1}^N \hat{\nabla}_i L$.

Computational cost. A single ZO estimate needs exactly *two forward passes* and does not store activations for backpropagation. MeZO keeps memory usage at the inference level by passing random *seeds* instead of full perturbation z . MeZO further observes that choosing $N > 1$ improves statistical stability but increases computation by a factor of N ; therefore it fixes $N = 1$.

From Classical ZO to ZO-SGD. Replacing the back-propagation gradient in SGD with the Classical ZO estimate gives the zeroth-order update $\theta_{t+1} = \theta_t - \eta_t \hat{\nabla} L(\theta_t; \mathcal{B}_t)$. MeZO realises this update in-place with the memory tricks above and serves as the baseline for our forthcoming improvements.

3.2 Fast Zeroth-Order Optimization

MeZO employs a fixed learning rate. Instead, FZOO dynamically tunes its step size using the standard deviation of loss values gathered from multiple forward passes within each mini-batch. For the enhanced computational efficiency, FZOO also incorporates a one-sided gradient estimation strategy and **we first utilize Rademacher random vectors for perturbations**. Letting u_1, \dots, u_N be N i.i.d Rademacher random vectors in \mathbb{R}^d , we construct our gradient estimation by function value queries

$$l_i = L(\theta_t + \epsilon u_i; \mathcal{B}_t), \quad \text{and} \quad l_0 = L(\theta_t; \mathcal{B}_t).$$

That is, the gradient estimate g_t is then computed by averaging N one-sided difference estimates

$$g_t = \frac{1}{\epsilon N} \sum_{i=1}^N (l_i - l_0) u_i. \quad (2)$$

The estimated variance σ_t^2 is computed as:

$$\sigma_t^2 = \frac{1}{N-1} \sum_{i=1}^N \left(l_i - \frac{1}{N} \sum_{j=1}^N l_j \right)^2. \quad (3)$$

Our FZOO updates the parameters according to equation 2 and equation 3:

$$\theta_{t+1} = \theta_t - \eta_t \frac{g_t}{\sigma_t}, \quad (4)$$

where η_t is the step size. The detailed implementation of FZOO is listed in Algorithm 1.

The equation 4 shows that FZOO receives larger steps at flat regions (where σ_t is small) and smaller steps at steep regions, mirroring Adam-style adaptivity while keeping memory at the inference level.

3.2.1 Motivation of FZOO

Adaptive first-order methods often estimate local curvature to scale updates. Similar adaptivity can be achieved by methods like normalized-SGD [2], which adjusts step sizes by normalizing the gradient, making it more memory-efficient compared to Adam. The parameter update follows normalized-SGD:

$$\theta_{t+1} = \theta_t - \eta_t \frac{g_t}{\|g_t\|}, \quad (5)$$

FZOO is inspired by normalized-SGD. Proposition 3.2 shows that $\sigma_t^2 = |g_t|^2 \cdot \epsilon^2 \cdot \frac{N-1}{N}$ which implies that FZOO is an extension of normalized-SGD to the ZO domain.

Variants. *FZOO-R* re-uses half of the losses from the previous mini-batch: $\sigma_t = \text{Std}(\{l_i^{\text{curr}}\} \cup \{l_i^{\text{prev}}\})$, achieving a full-batch variance estimate with only half the forward evaluations.

3.3 Efficient Implementation of Batched Forward Pass

The original ZO pipeline applies a perturbation and then runs a separate forward pass, which cannot take advantage of CUDA parallel computing. For layer j we split the computation into an unperturbed part $F^{(j)}$ and a perturbation part $P^{(j)}$. Using Gaussian noise forces two full matrix–vector products, so batching recovers little speed-up. Replacing the noise with a Rademacher vector $u_i \in \{\pm 1\}^d$ changes only the sign bits: $P^{(j)}$ is produced by a bit-level sign flip that degenerates into a single add / subtract, so the kernel issues additions instead of a second matrix–vector multiply, making it markedly faster because addition is cheaper than multiplication on CUDA cores [43].

Let X be the input and let $W^{(j)}$ denote the weight matrix of layer j . For the **first layer** we compute

$$F^{(1)} = W^{(1)} X, \quad Y_i^{(1)} = F^{(1)} + \epsilon (u_i \odot X), \quad i = 1, \dots, N,$$

and we stack the perturbed outputs along the batch dimension: $Y^{(1)} = [Y_1^{(1)}; \dots; Y_N^{(1)}]$.

Let $Y^{(j-1)}$ be the concatenated activations from the previous layer and $U = \text{diag}(u_1, \dots, u_N)$ the block-diagonal sign matrix that broadcasts the u_i across the batch axis. For **subsequent layers** ($j \geq 2$) we compute

$$F^{(j)} = W^{(j)} Y^{(j-1)}, \quad P^{(j)} = \epsilon (U \odot Y^{(j-1)}), \quad Y^{(j)} = F^{(j)} + P^{(j)}.$$

Because every layer’s N matrix multiplications are fused into a single CUDA kernel, wall-time drops by a factor p relative to sequential evaluation. Combining kernel fusion (p), Rademacher vector perturbations (r), and the one-sided estimator’s halved forward count (f) yields the overall speed-up

$$\boxed{f \times \min(s, r)}.$$

On OPT-125M with $N = 8$, our batched scheme($\min(s, r)$) delivers a $1.92\times$ speed-up over the “8 perturbations + 8 forward passes” baseline. Because the code still runs on vanilla transformers, even larger gains should be possible with high-throughput runtimes such as vLLM (section 4.4).

3.4 Equivalence to normalized-SGD

Proposition 3.2. *Let the stochastic gradient estimation g_t defined in equation 2 and the variance σ_t defined in equation 3. Then it holds that*

$$\mathbb{E} \left[\|g_t\|^2 \right] = \frac{N+d-1}{N} \|\nabla L(\theta_t, \mathcal{B}_t)\|^2 + \gamma_t \quad \text{and} \quad \gamma_t = O(\epsilon) \quad (6)$$

$$\mathbb{E} \left[\sigma_t^2 \right] = \epsilon^2 \cdot \|\nabla L(\theta_t, \mathcal{B}_t)\|^2 + \zeta_t \quad \text{with} \quad \zeta_t = O(\epsilon^3). \quad (7)$$

Remark 3.3. Comparing equation 7 and equation 6, and ignoring the perturbation terms ζ_t and γ_t (which are higher-order terms with respect to ϵ), we can obtain that:

$$\mathbb{E} \left[\|g_t\|^2 \right] = \frac{N+d-1}{N} \cdot \epsilon^{-2} \cdot \mathbb{E} \left[\sigma_t^2 \right]$$

Since $\frac{N+d-1}{N} \cdot \epsilon^{-2}$ is a constant independent of the iteration number, $\frac{g_t}{\sigma_t}$ can be regarded as a kind of normalized stochastic gradient, scaled by a constant factor. This theoretically establishes the connection between FZOO and normalized-SGD.

3.5 Convergence Analysis

Assumption 3.4. Suppose that the loss function $L(\theta)$ is \mathcal{L} -smooth, that is, for any $\theta_1, \theta_2 \in \mathbb{R}^d$, it holds that $L(\theta_2) \leq L(\theta_1) + \langle \nabla L(\theta_1), \theta_2 - \theta_1 \rangle + \frac{\mathcal{L}}{2} \|\theta_2 - \theta_1\|^2$.

Assumption 3.5 (Bounded Variance). The stochastic gradient $\nabla L(\theta, \mathcal{B})$ has bounded variance:

$$\mathbb{E} \left[\|\nabla L(\theta, \mathcal{B})\|^2 \right] \leq \|\nabla L(\theta)\|^2 + \mathcal{V}^2,$$

where \mathcal{V}^2 is a constant. The above is a standard assumption for stochastic gradient descent.

Theorem 3.6 (Convergence of FZOO). *Let the objective function $L(\theta)$ be \mathcal{L} -smooth, and Assumption 3.5 hold. The update rule is $\theta_{t+1} = \theta_t - \eta_t g_t$, where the effective step size $\eta_t = \frac{\eta}{\sigma_t}$ satisfies $\eta_t \leq \frac{N}{16d\mathcal{L}}$, and the learning rate factor η is set as $\eta = \left(\frac{L(\theta_1) - L(\theta^*)}{4d\mathcal{L}\mathcal{V}^2 \sum_{k=1}^T \sigma_k^{-2}} \right)^{1/2}$. Then, after T iterations, the FZOO algorithm satisfies:*

$$\begin{aligned} \frac{1}{T} \sum_{t=1}^T \mathbb{E} \left[\|\nabla L(\theta_t)\|^2 \right] &\leq \frac{64\sigma_* \left(d\mathcal{L}(L(\theta_1) - L(\theta^*)) \sum_{t=1}^T \sigma_t^{-2} \right)^{1/2}}{T} \\ &\quad + \frac{4\sigma_* \epsilon^2}{T} \left(\frac{d^3 \mathcal{L}^3}{8N} + \frac{Nd\mathcal{L}^3}{2} \right) \left(\frac{(L(\theta_1) - L(\theta^*)) \sum_{t=1}^T \sigma_t^{-2}}{4d\mathcal{L}\mathcal{V}^2} \right)^{1/2} \end{aligned}$$

where θ^* denotes the optimal solution (minimum) of $L(\theta)$, and $\sigma_* = \max_{t \in \{1, \dots, T\}} \sigma_t$.

This theorem shows that the FZOO algorithm converges to a stationary point whose gradient norm close to zero.

Table 1: Experiments on RoBERTa-large (350M parameters, k=16). All reported numbers are averaged accuracy across 5 runs. In notations like (2xM), M represents the memory overhead required for inference.

Task Type	SST-2	SST-5	SNLI	MNLI	RTE	TREC	Average
	sentiment		natural language inference			topic	
Zero-shot	79.0	35.5	50.2	48.8	51.4	32.0	49.5
LP	76.0	40.3	66.0	56.5	59.4	51.3	58.3
HiZOO (2xM)	93.2	46.2	74.6	64.9	66.8	79.8	70.9
ZO-Adam (3xM)	90.3	38.8	69.1	59.2	61.4	52.4	61.7
FT (6xM)	91.9	47.5	77.5	70.0	66.4	85.0	74.9
MeZO(prefix)	90.8	45.8	71.6	63.4	65.4	80.3	69.6
HiZOO(prefix)	92.3	47.2	68.8	61.6	65.4	82.0	69.6
FZOO(prefix)	92.9	43.7	70.8	67.0	64.6	82.8	70.3
MeZO	90.5	45.5	68.5	58.7	64.0	76.9	67.4
FZOO	93.3	47.6	75.9	64.9	67.9	78.8	71.4

4 Experiments

Large language models (LLMs) fall into two architectural families. Encoder–decoder models—BERT [12], ALBERT [21], etc.—tackle language understanding and are trained with a masked-token objective (Section 4.1). Decoder-only models—GPT [32, 3], OPT [47], LLaMA [40], Phi [23, 14], and others—focus on text generation and are trained autoregressively (Section 4.2). We benchmark FZOO under full-parameter fine-tuning on both model families, covering differentiable and non-differentiable tasks (Section 4.3), report its memory and wall-clock speed (Section 4.4), and compare it with standard ZO baselines (Section 4.5). Section 4.6 further shows that FZOO is complementary to parameter-efficient methods such as prefix-tuning [22].

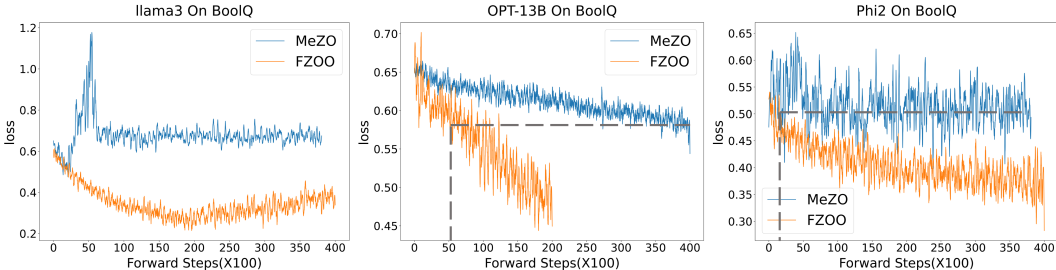


Figure 3: Training loss curves when using MeZO and FZOO to fine-tune different LLMs on the BoolQ dataset.

4.1 Masked Language Models

We perform experiments on the RoBERTa-large 350M model [25] across three NLP task paradigms: sentence classification, multiple choice and text generation. Following the experimental setup outlined in [28], we investigate both few-shot and many-shot settings, sampling k examples per class with $k = 16$ (results presented in Table 1) and $k = 512$ (results provided in Appendix D.1).

According to existing analysis, the cost of a single backpropagation is about three times that of a forward propagation [1], so the time required for each parameter update of Adam is equivalent to four forward propagations. Based on this, we plotted the loss curve in Figure 1. As can be seen from Figure 1, FZOO can reduce loss faster than MeZO, with an acceleration ratio of 18 times (with 1.92x parallel acceleration, it can potentially outperform Adam in wall-clock time). And its loss convergence speed is close to Adam, fully demonstrating FZOO’s excellent performance in training efficiency.

Table 1 shows that when optimizing the RoBERTa-large model with MeZO and FZOO, the performance of FZOO is on average **5.9%** higher than that of MeZO on multiple datasets across different NLP tasks. Specifically, FZOO outperforms MeZO more than **10.7%** in both the SNLI and MNLI dataset, showing comparable performance to HiZOO.

Table 2: Experiments on three different models (with 1000 examples) : Classification (SST-2, RTE, CB, BoolQ, WSC, WIC, MultiRC); Multiple Choice (COPA, ReCoRD); Generation (SQuAD, DROP). We highlight the best results between MeZO, HiZOO-L and FZOO in bold to facilitate comparison.

Model	Method	SST-2	RTE	CB	BoolQ	WSC	WIC	MultiRC	COPA	ReCoRD	SQuAD	DROP	Average
Phi-2	MeZO	86.6	67.1	75.0	72.4	59.6	54.4	78.2	86.0	71.7	85.7	37.8	70.7
Phi-2	HiZOO-L	88.9	68.9	75.2	72.0	62.4	59.2	79.2	86.0	72.1	85.7	36.2	71.4
Phi-2	FZOO	87.4	70.4	83.9	79.3	61.5	56.7	81.3	86.0	72.0	86.7	37.4	73.0
Llama3	MeZO	92.2	74.4	69.6	76.7	63.5	57.8	77.6	88.0	85.6	86.7	57.1	75.4
Llama3	HiZOO-L	94.3	75.1	69.6	77.1	63.5	57.7	77.9	89.0	85.6	87.7	49.4	75.2
Llama3	FZOO	94.3	77.6	69.6	81.8	65.4	60.8	81.5	88.0	85.3	87.9	56.5	77.2
OPT-13B	MeZO	91.4	66.1	66.0	67.6	63.5	59.4	57.3	88.0	81.7	84.7	30.9	68.8
OPT-13B	HiZOO-L	92.1	68.2	67.9	66.6	65.4	59.4	61.1	89.0	81.1	63.6	22.7	67.0
OPT-13B	FZOO	93.7	71.1	69.6	72.2	63.5	60.5	66.0	87.0	81.0	84.8	28.7	70.7

4.2 Auto-Regressive Language Models

Next, we expand the scope of our experiments by testing the Phi-2(2.7B), Llama3(8B) and OPT(13B) models on the same NLP tasks. The results of the experiment in Table 2 show that FZOO outperforms MeZO in most cases, with an average accuracy increase of **2.75%**. Aside from the ReCoRD and DROP datasets, FZOO surpasses MeZO in nearly all other cases.

FZOO significantly accelerates convergence speed during full-parameter tuning. As shown in Figure 3, FZOO not only achieves **8** \times speedup over MeZO on average in the context of full parameter tuning, but also has lower training loss. In addition, FZOO ultimately achieved a higher absolute accuracy improvement of **7.4%** than MeZO on the BoolQ task.

FZOO is able to adapt to large models with up to 66B parameters and maintains excellent performance. As shown in Table 3, on the OPT-66B model, FZOO outperforms MeZO with up to **13.2%** increase and **2.43%** increase on average.

4.3 Training with Non-Differentiable Objectives

Our proposed FZOO estimates the gradient by performing multiple forward propagation processes, so the objective function can be a non-differentiable function. Based on the MeZO [28] setup, we conduct some experiments using F1 as the optimization objective. As shown in Table 4, FZOO performs consistently well across OPT models of different scales, surpassing both MeZO and HiZOO-L, and achieving an average F1 improvement of **5.53%** over MeZO.

Table 3: Experiments on OPT-30B and OPT-66B (both use FT).

Task	SST-2	RTE	WSC	WIC	Average
30B MeZO	90.6	66.4	63.5	56.3	69.2
30B HiZOO-L	90.3	69.3	63.5	53.4	69.3
30B FZOO	91.2	69.3	63.5	60.2	71.1
66B MeZO	91.2	65.7	63.5	58.9	69.8
66B HiZOO-L	88.9	66.4	59.6	58.6	68.4
66B FZOO	93.6	74.4	58.6	59.2	71.5

Table 4: Non-differentiable optimization objectives (F1): Performance comparison on the SQuAD Task.

Model	OPT						
	Size	125M	1.3B	2.7B	6.7B	13B	Average
Zero-shot		9.7	27.2	29.9	36.6	46.2	29.9
MeZO		44.1	72.2	77.6	80.1	78.5	70.5
HiZOO-L		37.6	71.9	77.5	79.5	81.8	69.7
FZOO		51.0	74.6	81.8	79.8	84.7	74.4

4.4 Memory Usage and Time Efficiency Analysis

Memory Usage As shown in Figure 4, FZOO and MeZO have the same inference-level memory and do not need to store additional content like HiZOO. Even if Adam is trained with PEFT like prefix, it still requires several times more memory than FZOO.

Table 5: Wallclock time per step between Adam, MeZO and FZOO(N=8). See Appendix F for more.

Method	OPT-125M	RoBERTa-large	OPT-1.3B
Adam	0.1982s	0.3930s	0.5814s
MeZO	0.1368s	0.4305s	0.7218s
FZOO	0.3835s	0.6052s	1.6628s

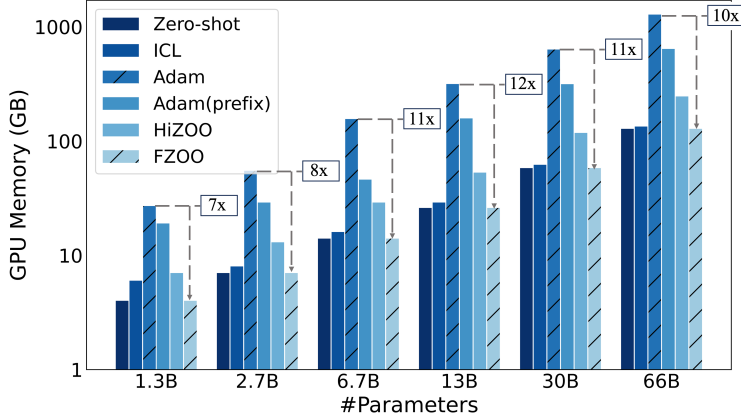


Figure 4: GPU memory consumption with different OPT models and tuning methods on MultiRC (400 tokens per example on average). More details can be found in Appendix E.

Table 6: Actual and potential speedup of FZOO for different tasks. Adam commonly achieves 20x speedup than MeZO.

Task(model)	SNLI (RoBERTa-large)	COPA (Phi-2)	WIC (OPT-13B)	CB (Llama3)
FZOO	20x	10x	9x	8x
Potential	40x	20x	18x	16x

Time Efficiency Adaptive step-size scheduling delivers up to $20\times$ speed-up in total steps over MeZO (Table 6). One FZOO step bundles 9 forward passes— $4.5\times$ more than MeZO—yet consumes only $3\times$ the wall-clock time (Appendix F), highlighting the gain from our parallel implementation.

4.5 Comparison with other ZO variants

We further compare FZOO with a wider range of ZO optimization methods [49]. As shown in Table 7, FZOO consistently outperforms all baselines. Compared to ZO-Adam, our FZOO achieves an average accuracy improvement of **5.77%** under full-parameter tuning, and **4.21%** under prefix-tuning, while using **40.5%** of the GPU memory.

Table 7: Performance comparison on SST2(Robert-Large and OPT-1.3B) and COPA(OPT-13B) using different ZO methods. Memory and runtime cost are multiples of ZO-SGD.

Model/Task	Roberts-Large		OPT-1.3B		OPT-13B		Average	Memory	Runtime
	FT	prefix	FT	prefix	FT	prefix			
ZO-SGD	89.4	90.0	90.8	91.4	90.0	79.0	88.4	1.0x	1.0x
ZO-SGD-MMT	89.6	89.1	85.2	91.2	87.0	85.0	87.8	1.56x	1.0x
ZO-SGD-Cons	89.6	89.1	88.3	88.1	82.0	84.0	86.8	1.0x	2.49x
ZO-SGD-Sign	52.5	53.6	87.2	89.5	80.0	78.0	73.4	1.0x	1.0x
ZO-Adam	89.8	90.2	84.4	91.4	82.0	79.0	86.1	2.47x	1.04x
HiZOO	93.2	92.7	90.7	91.4	88.0	87.0	90.5	2.04x	1.37x
HiZOO-L	92.5	92.7	90.7	91.4	88.0	87.0	90.4	1.12x	1.39x
FZOO	93.3	92.9	90.7	91.7	87.0	87.0	90.4	1.0x	0.56x

4.6 Orthogonality and Hyperparameter Analysis

Orthogonality to Fine-Tuning Strategies Our method is an optimization algorithm that focuses on how to update parameters, and is orthogonal to fine-tuning strategies that decide which parameters to update. We validate its compatibility by FT or Prefix on the roberta-large model.

Influence of the Number of Perturbations N per Step To further explore the trade-off between computational efficiency and convergence performance of the optimizer, we conducted a systematic evaluation on OPT-125M using the SST-2 dataset. As shown in Figure 6, increasing the number of perturbations N per step can improve accuracy under certain hyperparameter settings, but also raises per-step computational cost.

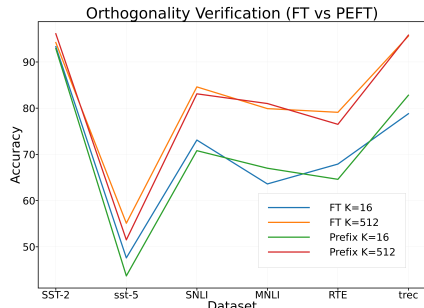


Figure 5: FZOO FT vs PEFT (prefix) on Roberta-large. We use FZOO (prefix) to fine-tune Roberta-large on multiple datasets. More results can be found in Appendix D.1.

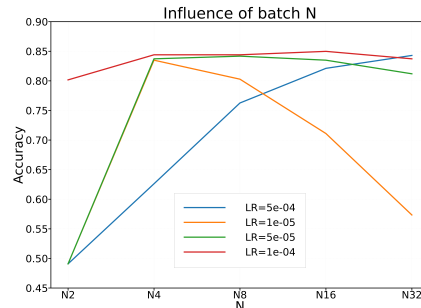


Figure 6: Accuracy Comparison under Different Perturbation Batch Sizes N for FT. The relevant experimental results are detailed in Appendix G.1.

5 Conclusion

We introduce FZOO, a novel zeroth-order optimizer achieving Adam-scale convergence speed for fine-tuning LLMs with inference-level memory. FZOO employs batched one-sided estimates and accelerated per-batch computations to significantly reduce forward passes. We provide theoretical analysis for its update rule and convergence. Experiments demonstrate FZOO converges in far fewer steps than MeZO, yielding superior performance across diverse LLMs. FZOO also seamlessly integrates with PEFT, enhancing practical fine-tuning.

References

- [1] Josh Alman and Zhao Song. The fine-grained complexity of gradient computation for training large language models. *arXiv preprint arXiv:2402.04497*, 2024.
- [2] Jeremy Bernstein, Yu-Xiang Wang, Kamyar Azizzadenesheli, and Animashree Anandkumar. signsgd: Compressed optimisation for non-convex problems. In *International Conference on Machine Learning*, pages 560–569. PMLR, 2018.
- [3] Tom B. Brown, Benjamin Mann, Nick Ryder, Melanie Subbiah, Jared Kaplan, Prafulla Dhariwal, Arvind Neelakantan, Pranav Shyam, Girish Sastry, Amanda Askell, Sandhini Agarwal, Ariel Herbert-Voss, Gretchen Krueger, Tom Henighan, Rewon Child, Aditya Ramesh, Daniel M. Ziegler, Jeffrey Wu, Clemens Winter, Christopher Hesse, Mark Chen, Eric Sigler, Mateusz Litwin, Scott Gray, Benjamin Chess, Jack Clark, Christopher Berner, Sam McCandlish, Alec Radford, Ilya Sutskever, and Dario Amodei. Language models are few-shot learners, 2020.
- [4] Hanqin Cai, Yuchen Lou, Daniel Mckenzie, and Wotao Yin. A zeroth-order block coordinate descent algorithm for huge-scale black-box optimization. In Marina Meila and Tong Zhang, editors, *Proceedings of the 38th International Conference on Machine Learning*, volume 139 of *Proceedings of Machine Learning Research*, pages 1193–1203. PMLR, 18–24 Jul 2021.
- [5] Minping Chen, You-Liang Huang, and Zeyi Wen. Towards efficient low-order hybrid optimizer for language model fine-tuning. 2025.
- [6] Pin-Yu Chen, Huan Zhang, Yash Sharma, Jinfeng Yi, and Cho-Jui Hsieh. Zoo: Zeroth order optimization based black-box attacks to deep neural networks without training substitute models. New York, NY, USA, 2017. Association for Computing Machinery.
- [7] Yiming Chen, Yuan Zhang, Liyuan Cao, Kun Yuan, and Zaiwen Wen. Enhancing zeroth-order fine-tuning for language models with low-rank structures. *arXiv preprint arXiv:2410.07698*, 2024.
- [8] Yiming Chen, Yuan Zhang, Yin Liu, Kun Yuan, and Zaiwen Wen. A memory efficient randomized subspace optimization method for training large language models. *arXiv preprint arXiv:2502.07222*, 2025.

- [9] Tim Dettmers, Mike Lewis, Younes Belkada, and Luke Zettlemoyer. GPT3.int8(): 8-bit matrix multiplication for transformers at scale. In *Advances in Neural Information Processing Systems*, 2022.
- [10] Tim Dettmers, Mike Lewis, Sam Shleifer, and Luke Zettlemoyer. 8-bit optimizers via block-wise quantization. In *International Conference on Learning Representations*, 2022.
- [11] Tim Dettmers, Artidoro Pagnoni, Ari Holtzman, and Luke Zettlemoyer. Qlora: Efficient finetuning of quantized llms, 2023.
- [12] Jacob Devlin, Ming-Wei Chang, Kenton Lee, and Kristina Toutanova. Bert: Pre-training of deep bidirectional transformers for language understanding. In *North American Chapter of the Association for Computational Linguistics*, 2019.
- [13] John Duchi, Elad Hazan, and Yoram Singer. Adaptive subgradient methods for online learning and stochastic optimization. *J. Mach. Learn. Res.*, 12(null):2121–2159, jul 2011.
- [14] Suriya Gunasekar, Yi Zhang, Jyoti Aneja, Caio César Teodoro Mendes, Allie Del Giorno, Sivakanth Gopi, Mojan Javaheripi, Piero Kauffmann, Gustavo de Rosa, Olli Saarikivi, Adil Salim, Shital Shah, Harkirat Singh Behl, Xin Wang, Sébastien Bubeck, Ronen Eldan, Adam Tauman Kalai, Yin Tat Lee, and Yuanzhi Li. Textbooks are all you need, 2023.
- [15] Wentao Guo, Jikai Long, Yimeng Zeng, Zirui Liu, Xinyu Yang, Yide Ran, Jacob R Gardner, Osbert Bastani, Christopher De Sa, Xiaodong Yu, et al. Zeroth-order fine-tuning of llms with extreme sparsity. *arXiv preprint arXiv:2406.02913*, 2024.
- [16] Suchin Gururangan, Ana Marasović, Swabha Swayamdipta, Kyle Lo, Iz Beltagy, Doug Downey, and Noah A. Smith. Don’t stop pretraining: Adapt language models to domains and tasks. In *Proceedings of the 58th Annual Meeting of the Association for Computational Linguistics*, pages 8342–8360, 2020.
- [17] Davood Hajinezhad and Michael M. Zavlanos. Gradient-free multi-agent nonconvex nonsmooth optimization. *2018 IEEE Conference on Decision and Control (CDC)*, pages 4939–4944, 2018.
- [18] Edward J Hu, yelong shen, Phillip Wallis, Zeyuan Allen-Zhu, Yuanzhi Li, Shean Wang, Lu Wang, and Weizhu Chen. LoRA: Low-rank adaptation of large language models. In *International Conference on Learning Representations*, 2022.
- [19] Shuoran Jiang, Qingcai Chen, Youchen Pan, Yang Xiang, Yukang Lin, Xiangping Wu, Chuanyi Liu, and Xiaobao Song. Zo-adamu optimizer: Adapting perturbation by the momentum and uncertainty in zeroth-order optimization, 2023.
- [20] Diederik Kingma and Jimmy Ba. Adam: A method for stochastic optimization. In *International Conference on Learning Representations (ICLR)*, San Diego, CA, USA, 2015.
- [21] Zhenzhong Lan, Mingda Chen, Sebastian Goodman, Kevin Gimpel, Piyush Sharma, and Radu Soricut. Albert: A lite bert for self-supervised learning of language representations. In *International Conference on Learning Representations*, 2020.
- [22] Xiang Lisa Li and Percy Liang. Prefix-tuning: Optimizing continuous prompts for generation. In Chengqing Zong, Fei Xia, Wenjie Li, and Roberto Navigli, editors, *Proceedings of the 59th Annual Meeting of the Association for Computational Linguistics and the 11th International Joint Conference on Natural Language Processing (Volume 1: Long Papers)*, pages 4582–4597, Online, August 2021. Association for Computational Linguistics.
- [23] Yuanzhi Li, Sébastien Bubeck, Ronen Eldan, Allie Del Giorno, Suriya Gunasekar, and Yin Tat Lee. Textbooks are all you need ii: phi-1.5 technical report, 2023.
- [24] Sijia Liu, Pin-Yu Chen, Xiangyi Chen, and Mingyi Hong. signsgd via zeroth-order oracle. In *International Conference on Learning Representations*, 2019.
- [25] Yinhan Liu, Myle Ott, Naman Goyal, Jingfei Du, Mandar Joshi, Danqi Chen, Omer Levy, Mike Lewis, Luke Zettlemoyer, and Veselin Stoyanov. Roberta: A robustly optimized bert pretraining approach. *arXiv preprint arXiv:1907.11692*, 2019.

- [26] Yong Liu, Zirui Zhu, Chaoyu Gong, Minhao Cheng, Cho-Jui Hsieh, and Yang You. Sparse mezo: Less parameters for better performance in zeroth-order llm fine-tuning. *arXiv preprint arXiv:2402.15751*, 2024.
- [27] Ilya Loshchilov and Frank Hutter. Decoupled weight decay regularization. In *International Conference on Learning Representations*, 2019.
- [28] Sadhika Malladi, Tianyu Gao, Eshaan Nichani, Alex Damian, Jason D. Lee, Danqi Chen, and Sanjeev Arora. Fine-tuning language models with just forward passes. In *Thirty-seventh Conference on Neural Information Processing Systems*, 2023.
- [29] Horia Mania, Aurelia Guy, and Benjamin Recht. Simple random search provides a competitive approach to reinforcement learning, 2018.
- [30] Long Ouyang, Jeffrey Wu, Xu Jiang, Diogo Almeida, Carroll Wainwright, Pamela Mishkin, Chong Zhang, Sandhini Agarwal, Katarina Slama, Alex Ray, et al. Training language models to follow instructions with human feedback. *Advances in Neural Information Processing Systems*, 35:27730–27744, 2022.
- [31] Rui Pan, Xiang Liu, Shizhe Diao, Renjie Pi, Jipeng Zhang, Chi Han, and Tong Zhang. Lisa: Layerwise importance sampling for memory-efficient large language model fine-tuning, 2024.
- [32] Alec Radford, Jeff Wu, Rewon Child, David Luan, Dario Amodei, and Ilya Sutskever. Language models are unsupervised multitask learners. 2019.
- [33] J.C. Spall. Multivariate stochastic approximation using a simultaneous perturbation gradient approximation. *IEEE Transactions on Automatic Control*, 37(3):332–341, 1992.
- [34] Tianxiang Sun, Zhengfu He, Hong Qian, Yunhua Zhou, Xuanjing Huang, and Xipeng Qiu. BBTv2: Towards a gradient-free future with large language models. In *Proceedings of the 2022 Conference on Empirical Methods in Natural Language Processing*, pages 3916–3930, 2022.
- [35] Tianxiang Sun, Yunfan Shao, Hong Qian, Xuanjing Huang, and Xipeng Qiu. Black-box tuning for language-model-as-a-service. In *International Conference on Machine Learning*, pages 20841–20855, 2022.
- [36] Yan Sun, Tiansheng Huang, Liang Ding, Li Shen, and Dacheng Tao. Tezo: Empowering the low-rankness on the temporal dimension in the zeroth-order optimization for fine-tuning llms. *arXiv preprint arXiv:2501.19057*, 2025.
- [37] Qitao Tan, Jun Liu, Zheng Zhan, Caiwei Ding, Yanzhi Wang, Jin Lu, and Geng Yuan. Harmony in divergence: Towards fast, accurate, and memory-efficient zeroth-order llm fine-tuning. *arXiv preprint arXiv:2502.03304*, 2025.
- [38] Xinyu Tang. *Effectively learning from data and generating data in differentially private machine learning*. PhD thesis, Princeton University, 2024.
- [39] Yujie Tang, Junshan Zhang, and Na Li. Distributed zero-order algorithms for nonconvex multiagent optimization. *IEEE Transactions on Control of Network Systems*, 8(1):269–281, 2021.
- [40] Hugo Touvron, Thibaut Lavril, Gautier Izacard, Xavier Martinet, Marie-Anne Lachaux, Timothée Lacroix, Baptiste Rozière, Naman Goyal, Eric Hambro, Faisal Azhar, Aurelien Rodriguez, Armand Joulin, Edouard Grave, and Guillaume Lample. Llama: Open and efficient foundation language models. *ArXiv*, abs/2302.13971, 2023.
- [41] Xiaoxing Wang, Xiaohan Qin, Xiaokang Yang, and Junchi Yan. ReLIZO: Sample reusable linear interpolation-based zeroth-order optimization. In *The Thirty-eighth Annual Conference on Neural Information Processing Systems*, 2024.
- [42] Yilong Wang, Haishan Ye, Yong Liu, Guang Dai, Ivor Tsang, and Jingdong Wang. The advancement in stochastic zeroth-order optimization: Mechanism of accelerated convergence of gaussian direction on objectives with skewed hessian eigenvalues.

- [43] Samuel Williams, Andrew Waterman, and David Patterson. Roofline: an insightful visual performance model for multicore architectures. *Communications of the ACM*, 52(4):65–76, 2009.
- [44] Haishan Ye, Zhichao Huang, Cong Fang, Chris Junchi Li, and Tong Zhang. Hessian-aware zeroth-order optimization for black-box adversarial attack, 2019.
- [45] Yang You, Jing Li, Sashank Reddi, Jonathan Hseu, Sanjiv Kumar, Srinadh Bhojanapalli, Xiaodan Song, James Demmel, Kurt Keutzer, and Cho-Jui Hsieh. Large batch optimization for deep learning: Training bert in 76 minutes. In *International Conference on Learning Representations*, 2020.
- [46] Matthew D. Zeiler. Adadelta: An adaptive learning rate method, 2012.
- [47] Susan Zhang, Stephen Roller, Naman Goyal, Mikel Artetxe, Moya Chen, Shuohui Chen, Christopher Dewan, Mona Diab, Xian Li, Xi Victoria Lin, Todor Mihaylov, Myle Ott, Sam Shleifer, Kurt Shuster, Daniel Simig, Punit Singh Koura, Anjali Sridhar, Tianlu Wang, and Luke Zettlemoyer. Opt: Open pre-trained transformer language models, 2022.
- [48] Yan Zhang, Yi Zhou, Kaiyi Ji, and Michael M. Zavlanos. A new one-point residual-feedback oracle for black-box learning and control. *Automatica*, 136(C), feb 2022.
- [49] Yihua Zhang, Pingzhi Li, Junyuan Hong, Jiaxiang Li, Yimeng Zhang, Wenqing Zheng, Pin-Yu Chen, Jason D. Lee, Wotao Yin, Mingyi Hong, Zhangyang Wang, Sijia Liu, and Tianlong Chen. Revisiting zeroth-order optimization for memory-efficient LLM fine-tuning: A benchmark. In Ruslan Salakhutdinov, Zico Kolter, Katherine Heller, Adrian Weller, Nuria Oliver, Jonathan Scarlett, and Felix Berkenkamp, editors, *Proceedings of the 41st International Conference on Machine Learning*, volume 235 of *Proceedings of Machine Learning Research*, pages 59173–59190. PMLR, 21–27 Jul 2024.
- [50] Huaqin Zhao, Jiayi Li, Yi Pan, Shizhe Liang, Xiaofeng Yang, Wei Liu, Xiang Li, Fei Dou, Tianming Liu, and Jin Lu. Helene: Hessian layer-wise clipping and gradient annealing for accelerating fine-tuning llm with zeroth-order optimization. *arXiv preprint arXiv:2411.10696*, 2024.
- [51] Jiawei Zhao, Zhenyu Zhang, Beidi Chen, Zhangyang Wang, Anima Anandkumar, and Yuandong Tian. Galore: Memory-efficient llm training by gradient low-rank projection. In *International Conference on Learning Representations*, 2024.
- [52] Yanjun Zhao, Sizhe Dang, Haishan Ye, Guang Dai, Yi Qian, and Ivor W. Tsang. Second-order fine-tuning without pain for llms: a hessian informed zeroth-order optimizer. In *International Conference on Learning Representations*, 2025.

A Related Works

A.1 First-order Optimizer Used in LLMs

In the development of deep learning, various optimization algorithms have been proposed to improve the efficiency and effectiveness of model training. Early methods include gradient descent (GD) and its improved versions, momentum method, Adagrad [13] and ADADELTA [46]. These methods have their own characteristics, but they have played an indispensable role in promoting technological progress in key fields such as computer vision. As the scale of models rapidly expands, the number of parameters surges, and the structure becomes increasingly complex, the applicability of traditional optimization methods in large model training has been severely tested. In this context, Adam has gradually become the mainstream choice for training and fine-tuning large-scale models due to its efficient convergence performance. To further improve the generalization ability, AdamW [27] was proposed. These optimizers have an implicit upper limit on batch size, and this bottleneck is particularly problematic in training large models. To address this phenomenon, LAMB [45] was proposed, which uses a principled layer-wise adaption strategy to accelerate the training of large-scale models under substantial batch sizes.

A.2 Zeroth-Order Optimizer

Zero-order optimization, also known as black-box optimization or derivative-free methods, has been widely explored in many studies in recent years, especially in single-point gradient estimation. Although these methods have their own characteristics, rough experiments conducted by [48] show that SPSA outperforms other methods.

Zeroth-Order Optimizer is widely used in situations where the objective function is difficult to express explicitly, or its gradient is impossible to obtain or extremely expensive to calculate. For example, derivative-free distributed algorithms have been proposed in [39, 17] to address nonconvex multi-agent optimization problems. A number of zero-order optimization methods, including ZO-BCD[4], ZOO[6], ZO-signSGD [24], and ZO-HessAware [44], are widely employed to generate black-box adversarial examples in deep learning.

MeZO [28] is the first to apply the classical ZO-SGD algorithm for fine-tuning large language models (LLMs), achieving competitive performance while significantly reducing memory usage and GPU time. This has led to a surge of follow-up works [19, 50, 26, 15, 38, 7, 42, 5, 37, 8, 36], which collectively establish zero-order optimization (ZOO) as a promising direction for LLM fine-tuning. Recently, HiZOO [52] further extends this line by being the first to incorporate diagonal Hessian information into ZOO for LLMs, enabling better handling of heterogeneous curvatures across different parameter dimensions and achieving improved convergence and performance.

B Detailed Convergence Analysis

B.1 Properties of Rademacher random vector

Lemma B.1. *Letting $x \in \mathbb{R}^d$ be a constant vector and $\{u_i\}_{i=1}^N$ be d -dimensional Rademacher random vectors, then it holds that*

$$\mathbb{E} \left[\left\| \sum_{i=1}^N u_i u_i^\top x \right\|^2 \right] = N(N + d - 1) \|x\|^2. \quad (8)$$

Proof. It holds that

$$\begin{aligned} \mathbb{E} \left[\left\| \sum_{i=1}^N u_i u_i^\top x \right\|^2 \right] &= \mathbb{E} \left[\sum_{i=1}^N \sum_{j=1}^N x^\top u_i u_i^\top u_j u_j^\top x \right] \\ &= \mathbb{E} \left[\sum_{j=1}^N x^\top u_j u_j^\top x \cdot \|u_j\|^2 \right] + \sum_{i \neq j} \langle \mathbb{E} [u_i u_i^\top x], \mathbb{E} [u_j u_j^\top x] \rangle \\ &= \mathbb{E} \left[\sum_{j=1}^N x^\top u_j u_j^\top x \cdot \|u_j\|^2 \right] + \sum_{i \neq j} \langle \mathbb{E} [u_i u_i^\top x], \mathbb{E} [u_j u_j^\top x] \rangle \\ &= Nd \|x\|^2 + (N^2 - N) \|x\|^2 \\ &= N(N + d - 1) \|x\|^2 \end{aligned}$$

□

Lemma B.2. *Letting u_i 's be Rademacher random vector, then it holds that*

$$\sum_{i=1}^N \mathbb{E} \left[\left\langle \nabla L(\theta, \mathcal{B}), u_i - \frac{1}{N} \sum_{j=1}^N u_j \right\rangle^2 \right] = (N - 1) \|\nabla L(\theta, \mathcal{B})\|^2. \quad (9)$$

Proof. It holds that

$$\sum_{i=1}^N \left\langle \nabla L(\theta, \mathcal{B}), u_i - \frac{1}{N} \sum_{j=1}^N u_j \right\rangle^2 \quad (10)$$

$$= \sum_{i=1}^N \langle \nabla L(\theta, \mathcal{B}), u_i \rangle^2 + N \left\langle \nabla L(\theta, \mathcal{B}), \frac{1}{N} \sum_{j=1}^N u_j \right\rangle^2 \quad (11)$$

$$- 2 \sum_{i=1}^N \langle \nabla L(\theta, \mathcal{B}), u_i \rangle \cdot \left\langle \nabla L(\theta, \mathcal{B}), \frac{1}{N} \sum_{j=1}^N u_j \right\rangle \quad (12)$$

$$= \sum_{i=1}^N \langle \nabla L(\theta, \mathcal{B}), u_i \rangle^2 - \frac{1}{N} \left\langle \nabla L(\theta, \mathcal{B}), \sum_{j=1}^N u_j \right\rangle^2 \quad (13)$$

Furthermore,

$$\begin{aligned}
\mathbb{E} \left[\left\langle \nabla L(\theta, \mathcal{B}), \sum_{j=1}^N u_j \right\rangle^2 \right] &= \sum_{i=1}^N \sum_{j=1}^N \langle \nabla L(\theta, \mathcal{B}), u_i \rangle \langle \nabla L(\theta, \mathcal{B}), u_j \rangle \\
&= \sum_{i=1}^N \mathbb{E} \left[\langle \nabla L(\theta, \mathcal{B}), u_i \rangle^2 \right] + \sum_{i \neq j} \mathbb{E} [\langle \nabla L(\theta, \mathcal{B}), u_i \rangle \langle \nabla L(\theta, \mathcal{B}), u_j \rangle] \\
&= \sum_{i=1}^N \mathbb{E} \left[\langle \nabla L(\theta, \mathcal{B}), u_i \rangle^2 \right] \\
&= dN \|\nabla L(\theta, \mathcal{B})\|^2.
\end{aligned}$$

Thus,

$$\sum_{j=1}^N \mathbb{E} \left[\left\langle \nabla L(\theta, \mathcal{B}), u_i - \frac{1}{N} \sum_{j=1}^N u_j \right\rangle^2 \right] = \left(1 - \frac{1}{N} \right) \sum_{i=1}^N \mathbb{E} \left[\langle \nabla L(\theta, \mathcal{B}), u_i \rangle^2 \right] = (N-1) \|\nabla L(\theta, \mathcal{B})\|^2.$$

□

B.2 Properties of g_t and σ_t

By the Taylor's expansion, we have

$$L(\theta + \epsilon u_i, \mathcal{B}) = L(\theta) + \epsilon \langle \nabla L(\theta, \mathcal{B}), u_i \rangle + \alpha(\theta, \epsilon u_i, \mathcal{B}) \quad (14)$$

where $\alpha(\theta, \epsilon u_i, \mathcal{B}) \triangleq L(\theta + \epsilon u_i, \mathcal{B}) - (L(\theta) + \epsilon \langle \nabla L(\theta, \mathcal{B}), u_i \rangle)$. By the \mathcal{L} -smoothness, we can obtain that

$$|\alpha(\theta, \epsilon u_i, \mathcal{B})| \leq \frac{\mathcal{L}\epsilon^2}{2} \|u_i\|^2 = \frac{d\mathcal{L}\epsilon^2}{2}, \quad (15)$$

where the last equality is because $u_i \in \{-1, +1\}$.

Lemma B.3. *Letting the estimated variance σ_t defined in equation 3, then, it holds that*

$$\mathbb{E} [\sigma^2] = \epsilon^2 \cdot \|\nabla L(\theta, \mathcal{B})\|^2 + \zeta, \quad (16)$$

with

$$\begin{aligned}
\zeta &= \frac{1}{N-1} \sum_{i=1}^N \left(\alpha(\theta, \epsilon u_i, \mathcal{B}) - \frac{1}{N} \sum_{j=1}^N \alpha(\theta, \epsilon u_j, \mathcal{B}) \right)^2 \\
&\quad + \epsilon \frac{1}{N-1} \sum_{i=1}^N \left\langle \nabla L(\theta, \mathcal{B}), u_i - \frac{1}{N} \sum_{j=1}^N u_j \right\rangle \cdot \left(\alpha(\theta, \epsilon u_i, \mathcal{B}) - \frac{1}{N} \sum_{j=1}^N \alpha(\theta, \epsilon u_j, \mathcal{B}) \right),
\end{aligned}$$

and

$$|\zeta| \leq \frac{Nd^2\mathcal{L}^2\epsilon^4}{2} + 2dN\mathcal{L}\epsilon^3 \cdot \|\nabla L(\theta, \mathcal{B})\|.$$

Proof. First, we have

$$\begin{aligned}
&L(\theta + \epsilon u_i, \mathcal{B}) - \frac{1}{N} \sum_{j=1}^N L(\theta + \epsilon u_j, \mathcal{B}) \\
&\stackrel{\text{equation 14}}{=} L(\theta) + \epsilon \langle \nabla L(\theta, \mathcal{B}), u_i \rangle + \alpha(\theta, \epsilon u_i, \mathcal{B}) - \frac{1}{N} \sum_{j=1}^N (L(\theta) + \epsilon \langle \nabla L(\theta, \mathcal{B}), u_j \rangle + \alpha(\theta, \epsilon u_j, \mathcal{B})) \\
&= \epsilon \left\langle \nabla L(\theta, \mathcal{B}), u_i - \frac{1}{N} \sum_{j=1}^N u_j \right\rangle + \alpha(\theta, \epsilon u_i, \mathcal{B}) - \frac{1}{N} \sum_{j=1}^N \alpha(\theta, \epsilon u_j, \mathcal{B}).
\end{aligned}$$

$$\begin{aligned}
& \sum_{i=1}^N \left(L(\theta + \epsilon u_i, \mathcal{B}) - \frac{1}{N} \sum_{j=1}^N L(\theta + \epsilon u_j, \mathcal{B}) \right)^2 \\
&= \sum_{i=1}^N \left(\epsilon \left\langle \nabla L(\theta, \mathcal{B}), u_i - \frac{1}{N} \sum_{j=1}^N u_j \right\rangle + \beta_i \right)^2 \\
&= \sum_{i=1}^N \left(\epsilon^2 \left\langle \nabla L(\theta, \mathcal{B}), u_i - \frac{1}{N} \sum_{j=1}^N u_j \right\rangle^2 + \beta_i^2 + \epsilon \left\langle \nabla L(\theta, \mathcal{B}), u_i - \frac{1}{N} \sum_{j=1}^N u_j \right\rangle \beta_i \right),
\end{aligned}$$

where we use $\beta_i \triangleq \alpha(\theta, \epsilon u_i, \mathcal{B}) - \frac{1}{N} \sum_{j=1}^N \alpha(\theta, \epsilon u_j, \mathcal{B})$.

Furthermore, it holds that

$$\sum_{i=1}^N \beta_i^2 = \left(1 - \frac{1}{N}\right) \sum_{i=1}^N \alpha^2(\theta, \epsilon u_i, \mathcal{B}) \leq \frac{Nd^2 \mathcal{L}^2 \epsilon^4}{4},$$

and

$$\sum_{i=1}^N \left| \left\langle \nabla L(\theta, \mathcal{B}), u_i - \frac{1}{N} \sum_{j=1}^N u_j \right\rangle \beta_i \right| \leq N \left\| \left\langle \nabla L(\theta, \mathcal{B}), u_i - \frac{1}{N} \sum_{j=1}^N u_j \right\rangle \right\| \|\beta_i\| \stackrel{\text{equation 15}}{\leq} dN \mathcal{L} \epsilon^2 \|\nabla L(\theta, \mathcal{B})\|.$$

Therefore, we can obtain that

$$\mathbb{E}[\sigma^2] = \frac{1}{N-1} \sum_{i=1}^N \left(\epsilon^2 \left\langle \nabla L(\theta, \mathcal{B}), u_i - \frac{1}{N} \sum_{j=1}^N u_j \right\rangle^2 + \beta_i^2 + \epsilon \left\langle \nabla L(\theta, \mathcal{B}), u_i - \frac{1}{N} \sum_{j=1}^N u_j \right\rangle \beta_i \right)$$

$$\stackrel{\text{equation 9}}{=} \epsilon^2 \cdot \|\nabla L(\theta, \mathcal{B})\|^2 + \zeta$$

Finally, we have

$$\begin{aligned}
|\zeta| &\leq \frac{1}{N-1} \sum_{i=1}^N \beta_i^2 + \epsilon \frac{1}{N-1} \sum_{i=1}^N \left| \left\langle \nabla L(\theta, \mathcal{B}), u_i - \frac{1}{N} \sum_{j=1}^N u_j \right\rangle \beta_i \right| \\
&\leq \frac{Nd^2 \mathcal{L}^2 \epsilon^4}{2} + 2dN \mathcal{L} \epsilon^3 \cdot \|\nabla L(\theta, \mathcal{B})\|.
\end{aligned}$$

□

Lemma B.4. *Letting the stochastic gradient estimation g_t defined in equation 2, then it satisfies the following properties*

$$g_t = \frac{1}{N} \sum_{i=1}^N u_i u_i^\top \nabla L(\theta_t, \mathcal{B}_t) + \tau_t \quad (17)$$

with

$$\tau_t = \frac{1}{N} \sum_{i=1}^N \epsilon^{-1} \alpha(\theta, \epsilon u_i, \mathcal{B}) \cdot u_i \text{ and } \mathbb{E}[\tau_t^2] \leq \frac{d^3 \mathcal{L}^2 \epsilon^2}{4N}. \quad (18)$$

Proof. By the definition of g_t in equation 2, we can obtain that

$$\begin{aligned}
g_t &\stackrel{\text{equation 2}}{=} \frac{1}{N} \sum_{i=1}^N \frac{L(\theta + \epsilon u_i, \mathcal{B}) - L(\theta, \mathcal{B})}{\epsilon} u_i \\
&\stackrel{\text{equation 14}}{=} \frac{1}{N} \sum_{i=1}^N u_i u_i^\top \nabla L(\theta, \mathcal{B}) + \frac{1}{N} \sum_{i=1}^N \epsilon^{-1} \alpha(\theta, \epsilon u_i, \mathcal{B}) \cdot u_i \\
&= \frac{1}{N} \sum_{i=1}^N u_i u_i^\top \nabla L(\theta, \mathcal{B}) + \tau_t.
\end{aligned}$$

Furthermore,

$$\begin{aligned}\mathbb{E}[\tau^2] &= \frac{1}{N^2} \sum_{i=1}^N \mathbb{E} \left[(\epsilon^{-1} \alpha(\theta, \epsilon u_i, \mathcal{B}))^2 \cdot \|u_i\|^2 \right] \\ &= \frac{d\epsilon^{-2}}{N} \mathbb{E} [\alpha^2(\theta, \epsilon u_j, \mathcal{B})] \stackrel{\text{equation 15}}{\leq} \frac{d^3 \mathcal{L}^2 \epsilon^2}{4N}.\end{aligned}$$

□

Lemma B.5. *Letting the stochastic gradient estimation g_t defined in equation 2, then its norm satisfies that*

$$\mathbb{E} [\|g_t\|^2] = \frac{N+d-1}{N} \|\nabla L(\theta_t, \mathcal{B}_t)\|^2 + \gamma_t, \quad (19)$$

with

$$\begin{aligned}\gamma_t &= \frac{d\epsilon^{-2}}{N} \mathbb{E} [\alpha^2(\theta, \epsilon u_j, \mathcal{B})] + \frac{d\epsilon^{-1}}{N} \mathbb{E} [u_i^\top \nabla L(\theta, \mathcal{B}) \alpha(\theta, \epsilon u_i, \mathcal{B})] \\ &\quad + \frac{(N-1)\epsilon^{-1}}{N} \langle \nabla L(\theta, \mathcal{B}), \mathbb{E} [\alpha(\theta, \epsilon u_j, \mathcal{B}) \cdot u_j] \rangle.\end{aligned}$$

Furthermore, it holds that

$$|\gamma_t| \leq \frac{d^3 \mathcal{L}^2 \epsilon^2}{4N} + d^2 \mathcal{L} \|\nabla L(\theta_t, \mathcal{B}_t)\| \cdot \epsilon.$$

Proof. First, we have

$$\begin{aligned}\|g_t\|^2 &= \frac{1}{N^2} \left\| \sum_{i=1}^N u_i u_i^\top \nabla L(\theta, \mathcal{B}) \right\|^2 + \frac{1}{N^2} \sum_{i=1}^N (\epsilon^{-1} \alpha(\theta, \epsilon u_i, \mathcal{B}))^2 \cdot \|u_i\|^2 \\ &\quad + \frac{1}{N^2} \sum_{i=1}^N \sum_{j=1}^N \langle u_i u_i^\top \nabla L(\theta, \mathcal{B}), \epsilon^{-1} \alpha(\theta, \epsilon u_j, \mathcal{B}) \cdot u_j \rangle \\ &= \frac{1}{N^2} \left\| \sum_{i=1}^N u_i u_i^\top \nabla L(\theta, \mathcal{B}) \right\|^2 + \frac{d}{N^2} \sum_{i=1}^N (\epsilon^{-1} \alpha(\theta, \epsilon u_i, \mathcal{B}))^2 \\ &\quad + \frac{1}{N^2} \sum_{i=1}^N \sum_{j=1}^N \langle u_i u_i^\top \nabla L(\theta, \mathcal{B}), \epsilon^{-1} \alpha(\theta, \epsilon u_j, \mathcal{B}) \cdot u_j \rangle.\end{aligned}$$

We also have

$$\mathbb{E} \left[\left\| \sum_{i=1}^N u_i u_i^\top \nabla L(\theta, \mathcal{B}) \right\|^2 \right] = N(N+d-1) \|\nabla L(\theta, \mathcal{B})\|^2.$$

Furthermore, it holds that

$$\begin{aligned}&\mathbb{E} \left[\sum_{i=1}^N \sum_{j=1}^N \langle u_i u_i^\top \nabla L(\theta, \mathcal{B}), \epsilon^{-1} \alpha(\theta, \epsilon u_j, \mathcal{B}) \cdot u_j \rangle \right] \\ &= \mathbb{E} \left[\sum_{i=1}^N \langle u_i u_i^\top \nabla L(\theta, \mathcal{B}), \alpha(\theta, \epsilon u_i, \mathcal{B}) \cdot u_i \rangle \right] + \mathbb{E} \left[\sum_{i \neq j}^N \langle u_i u_i^\top \nabla L(\theta, \mathcal{B}), \epsilon^{-1} \alpha(\theta, \epsilon u_j, \mathcal{B}) \cdot u_j \rangle \right] \\ &= N d \epsilon^{-1} \mathbb{E} [u_i^\top \nabla L(\theta, \mathcal{B}) \alpha(\theta, \epsilon u_i, \mathcal{B})] + N(N-1) \epsilon^{-1} \langle \nabla L(\theta, \mathcal{B}), \mathbb{E} [\alpha(\theta, \epsilon u_j, \mathcal{B}) \cdot u_j] \rangle.\end{aligned}$$

Thus,

$$\begin{aligned}\mathbb{E} [\|g_t\|^2] &= \frac{N+d-1}{N} \|\nabla L(\theta, \mathcal{B})\|^2 + \frac{d\epsilon^{-2}}{N} \mathbb{E} [\alpha^2(\theta, \epsilon u_j, \mathcal{B})] \\ &\quad + \frac{d\epsilon^{-1}}{N} \mathbb{E} [u_i^\top \nabla L(\theta, \mathcal{B}) \alpha(\theta, \epsilon u_i, \mathcal{B})] + \frac{(N-1)\epsilon^{-1}}{N} \langle \nabla L(\theta, \mathcal{B}), \mathbb{E} [\alpha(\theta, \epsilon u_j, \mathcal{B}) \cdot u_j] \rangle.\end{aligned}$$

Finally,

$$\begin{aligned}
|\gamma_t| &\leq \frac{d\epsilon^{-2}}{N} |\mathbb{E} [\alpha^2(\theta, \epsilon u_j, \mathcal{B})]| + \frac{d\epsilon^{-1}}{N} |\mathbb{E} [u_i^\top \nabla L(\theta, \mathcal{B}) \alpha(\theta, \epsilon u_i, \mathcal{B})]| \\
&\quad + \frac{(N-1)\epsilon^{-1}}{N} |\langle \nabla L(\theta, \mathcal{B}), \mathbb{E} [\alpha(\theta, \epsilon u_j, \mathcal{B}) \cdot u_j] \rangle| \\
&\stackrel{\text{equation 15}}{\leq} \frac{d\epsilon^{-2}}{N} \cdot \frac{d^2 \mathcal{L}^2 \epsilon^4}{4} + \frac{d\epsilon^{-1}}{N} \|\nabla L(\theta_t, \mathcal{B}_t)\| \cdot \frac{d\mathcal{L}\epsilon^2}{2} + \epsilon^{-1} \|\nabla L(\theta_t, \mathcal{B}_t)\| \cdot \frac{d\mathcal{L}\epsilon^2}{2} \cdot d^{1/2} \\
&= \frac{d^3 \mathcal{L}^2 \epsilon^2}{4N} + \left(\frac{d^2 \mathcal{L}\epsilon}{2N} + \frac{d^{3/2} \mathcal{L}\epsilon}{2} \right) \|\nabla L(\theta_t, \mathcal{B}_t)\| \\
&\leq \frac{d^3 \mathcal{L}^2 \epsilon^2}{4N} + d^2 \mathcal{L} \|\nabla L(\theta_t, \mathcal{B}_t)\| \cdot \epsilon,
\end{aligned}$$

which concludes the proof. \square

B.3 Proof of Proposition 3.2

Proof. Lemma B.3 and Lemma B.3 imply the result of Proposition 3.2. \square

B.4 Proof of Theorem 3.6

Proof. First, we have

$$\mathbb{E} [\langle \nabla L(\theta_t), -\tau_t \rangle] \leq \frac{\|\nabla L(\theta_t)\|^2 + \mathbb{E} \|\tau_t\|^2}{2} \stackrel{\text{equation 18}}{\leq} \frac{\|\nabla L(\theta_t)\|^2}{2} + \frac{d^3 \mathcal{L}^2 \epsilon^2}{8N}, \quad (20)$$

where the first inequality is because of the Cauchy's inequality.

It also holds that

$$d\mathcal{L}^2 \sigma_t^{-2} \eta^2 \epsilon \cdot \|\nabla L(\theta_t, \mathcal{B}_t)\| \leq \frac{2d\mathcal{L}\sigma_t^{-2} \eta^2 \|\nabla L(\theta_t, \mathcal{B}_t)\|^2}{N} + \frac{Nd\mathcal{L}^3 \sigma_t^{-2} \eta^2 \epsilon^2}{2}. \quad (21)$$

Thus, by the \mathcal{L} -smoothness of $\nabla L(\theta)$, we have

$$\begin{aligned}
\mathbb{E} [L(\theta_{t+1})] &\leq L(\theta_t) - \eta\sigma_t^{-1} \mathbb{E} [\langle \nabla L(\theta_t), g_t \rangle] + \frac{\mathcal{L}\sigma_t^{-2} \eta^2}{2} \mathbb{E} [\|g_t\|^2] \\
&\stackrel{\text{equation 17}}{=} L(\theta_t) - \eta\sigma_t^{-1} \mathbb{E} \left[\left\langle \nabla L(\theta_t), \frac{1}{N} \sum_{i=1}^N u_i u_i^\top \nabla L(\theta_t, \mathcal{B}_t) + \tau_t \right\rangle \right] + \frac{\mathcal{L}\sigma_t^{-2} \eta^2}{2} \mathbb{E} [\|g_t\|^2] \\
&= L(\theta_t) - \eta\sigma_t^{-1} \|\nabla L(\theta_t)\|^2 + \eta\sigma_t^{-1} \mathbb{E} [\langle \nabla L(\theta_t), -\tau_t \rangle] + \frac{\mathcal{L}\sigma_t^{-2} \eta^2}{2} \mathbb{E} [\|g_t\|^2] \\
&\stackrel{\text{equation 20}}{\leq} \stackrel{\text{equation 6}}{=} L(\theta_t) - \frac{\eta\sigma_t^{-1}}{2} \|\nabla L(\theta_t)\|^2 + \frac{\eta\sigma_t^{-1} d^3 \mathcal{L}^2 \epsilon^2}{8N} + \frac{N+d-1}{N} \cdot \frac{\mathcal{L}\sigma_t^{-2} \eta^2}{2} \|\nabla L(\theta_t, \mathcal{B}_t)\|^2 \\
&\quad + \frac{d^3 \mathcal{L}^3 \sigma_t^{-2} \eta^2 \epsilon^2}{8N} + d\mathcal{L}^2 \sigma_t^{-2} \eta^2 \epsilon \cdot \|\nabla L(\theta_t, \mathcal{B}_t)\| \\
&\stackrel{\text{equation 21}}{\leq} L(\theta_t) - \frac{\eta\sigma_t^{-1}}{2} \|\nabla L(\theta_t)\|^2 + \frac{\eta\sigma_t^{-1} d^3 \mathcal{L}^2 \epsilon^2}{8N} + \frac{2d\mathcal{L}\sigma_t^{-2} \eta^2}{N} \cdot \|\nabla L(\theta_t, \mathcal{B}_t)\|^2 \\
&\quad + \frac{d^3 \mathcal{L}^3 \sigma_t^{-2} \eta^2 \epsilon^2}{8N} + \frac{2d\mathcal{L}\sigma_t^{-2} \eta^2 \|\nabla L(\theta_t, \mathcal{B}_t)\|^2}{N} + \frac{Nd\mathcal{L}^3 \sigma_t^{-2} \eta^2 \epsilon^2}{2} \\
&\stackrel{\text{equation 3}}{\leq} L(\theta_t) - \frac{\eta\sigma_t^{-1}}{2} \|\nabla L(\theta_t)\|^2 + \frac{4d\mathcal{L}\sigma_t^{-2} \eta^2}{N} \|\nabla L(\theta_t)\|^2 + \frac{4d\mathcal{L}\sigma_t^{-2} \eta^2 \mathcal{V}^2}{N} \\
&\quad + \frac{d^3 \mathcal{L}^3 \sigma_t^{-2} \eta^2 \epsilon^2}{8N} + \frac{Nd\mathcal{L}^3 \sigma_t^{-2} \eta^2 \epsilon^2}{2} \\
&\leq L(\theta_t) - \frac{\eta\sigma_t^{-1}}{4} \|\nabla L(\theta_t)\|^2 + \frac{4d\mathcal{L}\sigma_t^{-2} \eta^2 \mathcal{V}^2}{N} + \frac{d^3 \mathcal{L}^3 \sigma_t^{-2} \eta^2 \epsilon^2}{8N} + \frac{Nd\mathcal{L}^3 \sigma_t^{-2} \eta^2 \epsilon^2}{2},
\end{aligned}$$

where the last inequality is because of step size satisfies $\eta\sigma_t^{-1} \leq \frac{N}{16d\mathcal{L}}$.

We can represent above equation as follows:

$$\frac{\eta\sigma_t^{-1}}{4}\mathbb{E}\left[\|\nabla L(\theta_t)\|^2\right] \leq \mathbb{E}[L(\theta_t) - L(\theta_{t+1})] + \frac{4d\mathcal{L}\sigma_t^{-2}\eta^2\mathcal{V}^2}{N} + \frac{d^3\mathcal{L}^3\sigma_t^{-2}\eta^2\epsilon^2}{8N} + \frac{Nd\mathcal{L}^3\sigma_t^{-2}\eta^2\epsilon^2}{2}.$$

Telescoping above equation, we can obtain that

$$\frac{1}{T}\sum_{t=1}^T\frac{\eta\sigma_t^{-1}}{4}\mathbb{E}\left[\|\nabla L(\theta_t)\|^2\right] \leq \frac{L(\theta_1) - L(\theta^*)}{T} + \sum_{t=1}^T\left(\frac{4d\mathcal{L}\sigma_t^{-2}\eta^2\mathcal{V}^2}{TN} + \frac{d^3\mathcal{L}^3\sigma_t^{-2}\eta^2\epsilon^2}{8TN} + \frac{Nd\mathcal{L}^3\sigma_t^{-2}\eta^2\epsilon^2}{2T}\right)$$

$$\begin{aligned} \frac{1}{T}\sum_{t=1}^T\mathbb{E}\left[\|\nabla L(\theta_t)\|^2\right] &\leq \frac{1}{T}\sum_{t=1}^T\frac{\sigma_t^{-1}}{\sigma_*^{-1}}\mathbb{E}\left[\|\nabla L(\theta_t)\|^2\right] \\ &\leq \frac{4\sigma_*(L(\theta_1) - L(\theta^*))}{\eta T} + 4\sigma_*\sum_{t=1}^T\left(\frac{4d\mathcal{L}\sigma_t^{-2}\eta\mathcal{V}^2}{TN} + \frac{d^3\mathcal{L}^3\sigma_t^{-2}\eta\epsilon^2}{8TN} + \frac{Nd\mathcal{L}^3\sigma_t^{-2}\eta\epsilon^2}{2T}\right) \end{aligned}$$

By setting

$$\eta = \left(\frac{L(\theta_1) - L(\theta^*)}{4d\mathcal{L}\mathcal{V}^2\sum_{t=1}^T\sigma_t^{-2}}\right)^{1/2},$$

we can obtain that

$$\begin{aligned} \frac{1}{T}\sum_{t=1}^T\mathbb{E}\left[\|\nabla L(\theta_t)\|^2\right] &\leq \frac{64\sigma_*\left(d\mathcal{L}(L(\theta_1) - L(\theta^*))\sum_{t=1}^T\sigma_t^{-2}\right)^{1/2}}{T} \\ &\quad + \frac{4\sigma_*\epsilon^2}{T}\left(\frac{d^3\mathcal{L}^3}{8N} + \frac{Nd\mathcal{L}^3}{2}\right)\left(\frac{(L(\theta_1) - L(\theta^*))\sum_{t=1}^T\sigma_t^{-2}}{4d\mathcal{L}\mathcal{V}^2}\right)^{1/2} \end{aligned}$$

$$\eta\sigma_t^{-1} \leq \frac{N}{16d\mathcal{L}}$$

Accordingly, we can obtain that

$$\mathbb{E}[L(\theta_{t+1})] \leq L(\theta_t) - \frac{\eta\sigma_t^{-1}}{4}\|\nabla L(\theta_t)\|^2 + \frac{4d\mathcal{L}\sigma_t^{-2}\eta^2\mathcal{V}^2}{N} + \frac{d^3\mathcal{L}^3\sigma_t^{-2}\eta^2\epsilon^2}{8N} + \frac{Nd\mathcal{L}^3\sigma_t^{-2}\eta^2\epsilon^2}{2}.$$

□

Algorithm 2 FZOO-R

Require: parameters $\theta \in \mathbb{R}^d$, loss $L : \mathbb{R}^d \rightarrow \mathbb{R}$, step budget T , perturbation scale ϵ , batch size N , learning rate schedule $\{\eta_t\}$

- 1: Initialize $l_{-1} \leftarrow \emptyset$ ▷ To store previous losses
- 2: **for** $t = 1, \dots, T$ **do**
- 3: $\ell, \theta, seeds \leftarrow \text{BatchPerturbParameters}(\theta, \epsilon, N)$
- 4: **if** l_{-1} is not empty **then**
- 5: $std \leftarrow$ standard deviation of $\text{concat}(\ell, l_{-1})$
- 6: **else**
- 7: $std \leftarrow$ standard deviation of ℓ
- 8: **end if**
- 9: $projected_grad \leftarrow (\ell - \mathcal{L}(\theta; \mathcal{B})) / (N * std)$
- 10: $l_{-1} \leftarrow \ell$ ▷ Save the current loss
- 11: $\text{BatchUpdateParameter}(projected_grad, seeds, \theta, \eta_t)$
- 12: **end for**
- 13: **function** BATCHPERTURBPARAMETER(θ, ϵ, N)
- 14: Sample batch $\mathcal{B} \subset \mathcal{D}$; obtain input X and first layer weights $W^{(1)}$
- 15: Initialize random seeds $seeds \leftarrow \{s_1, \dots, s_N\}$
- 16: Generate perturbation vectors $u \in \{\pm 1\}^{N \times d}$ using $seeds$
- 17: Compute unperturbed activations $F^{(1)} \leftarrow W^{(1)}X$
- 18: Compute perturbed activations: $Y_i^{(1)} \leftarrow F^{(1)} + \epsilon(u_i \odot X)$, $i = 1, \dots, N$
- 19: Concatenate activations $Y^{(1)} \leftarrow [Y_1^{(1)}; \dots; Y_N^{(1)}]$
- 20: **for** $j = 2, 3, \dots$ **do**
- 21: $F^{(j)} \leftarrow W^{(j)}Y^{(j-1)}$ ▷ Compute unperturbed activations at layer j
- 22: $P^{(j)} \leftarrow \epsilon(u \odot Y^{(j-1)})$ ▷ Compute perturbations at layer j
- 23: $Y^{(j)} \leftarrow F^{(j)} + P^{(j)}$ ▷ Compute perturbed activations in parallel at layer j
- 24: **end for**
- 25: $\ell \leftarrow \mathcal{L}(Y^{(final)}; \mathcal{B})$ ▷ Compute final losses in parallel
- 26: **return** $\ell, \theta, seeds$
- 27: **end function**
- 28: **function** BATCHUPDATEPARAMETER($projected_grad, seeds, \theta, \eta$)
- 29: **for** $idx, s \in \text{enumerate}(seeds)$ **do**
- 30: Reset random number generator with seed s ▷ For sampling u
- 31: **for** $\theta_i \in \theta$ **do**
- 32: $u \sim \text{Uniform}(\{+1, -1\})$
- 33: $\theta_i \leftarrow \theta_i - \eta * projected_grad_{idx} * u$
- 34: **end for**
- 35: **end for**
- 36: **end function**

C FZOO Variants

C.1 FZOO-R

Although FZOO accelerates training convergence through adaptive step size adjustment, each update requires multiple forward passes. To reduce the computational overhead per update, we propose a loss reuse variant FZOO-R. Instead of performing the full recommended number of forward passes for each update, we halve it. FZOO-R estimates the gradient direction solely based on these few forward passes, while reusing loss values from the previous update to adjust the step size. The detailed procedure is described in Algorithm 2. We visualize the loss curves of FZOO-R and FZOO in Figure 7. On most datasets, FZOO-R achieves comparable convergence to FZOO while requiring only half the update time per step.

C.2 FZOO without parallel

To facilitate controlled evaluation, we release a *non-parallel* variant of FZOO, allowing for a clearer comparison of the total step-count reduction ratio against baselines such as MeZO, as illustrated in Al-

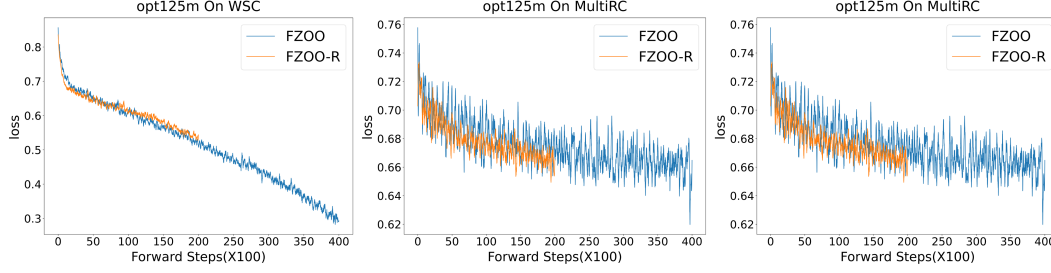


Figure 7: Loss curves on opt-125m between FZOO and FZOO-R.

Algorithm 3 FZOO without parallel

Require: parameters $\theta \in \mathbb{R}^d$, loss $L : \mathbb{R}^d \rightarrow \mathbb{R}$, step budget T , perturbation scale ϵ , batch size N , learning rate schedule $\{\eta_t\}$

- 1: **for** $t = 1, \dots, T$ **do**
- 2: $\ell, \theta, seeds \leftarrow \text{BatchPerturbParameters}(\theta, \epsilon, N)$
- 3: $std \leftarrow$ standard deviation of ℓ
- 4: $projected_grad \leftarrow (\ell - \mathcal{L}(\theta; \mathcal{B})) / (N * std)$
- 5: $\text{BatchUpdateParameter}(projected_grad, seeds, \theta, \eta_t)$
- 6: **end for**
- 7: **function** BATCHPERTURBPARAMETER(θ, ϵ, N)
- 8: Sample batch $\mathcal{B} \subset \mathcal{D}$
- 9: **for** $i = 1, \dots, N$ **do**
- 10: Sample random seed s and append to $seeds$
- 11: $\theta \leftarrow \text{PerturbParameters}(\theta, \epsilon, s)$
- 12: Append $\mathcal{L}(\theta; \mathcal{B})$ to ℓ
- 13: $\theta \leftarrow \text{PerturbParameters}(\theta, -\epsilon, s)$ \triangleright Reset parameters before next forward pass
- 14: **end for**
- 15: **return** $\ell, \theta, seeds$
- 16: **end function**
- 17: **function** PERTURBPARAMETER(θ, ϵ, s)
- 18: Reset random number generator with seed s \triangleright For sampling u
- 19: **for** $\theta_i \in \theta$ **do**
- 20: $u \sim \text{Uniform}(\{+1, -1\})$
- 21: $\theta_i \leftarrow \theta_i + \epsilon u$ \triangleright Modify parameters in place
- 22: **end for**
- 23: **return** θ
- 24: **end function**
- 25: **function** BATCHUPDATEPARAMETER($projected_grad, seeds, \theta, \eta$)
- 26: **for** $idx, s \in \text{enumerate}(seeds)$ **do**
- 27: Reset random number generator with seed s \triangleright For sampling u
- 28: **for** $\theta_i \in \theta$ **do**
- 29: $u \sim \text{Uniform}(\{+1, -1\})$
- 30: $\theta_i \leftarrow \theta_i - \eta * projected_grad_{idx} * u$
- 31: **end for**
- 32: **end for**
- 33: **end function**

gorithm 3. In this version, the perturbation noise is sampled from a Rademacher random vector (± 1), ensuring that, apart from the removal of parallel optimization, all other components remain identical to the original FZOO. **Note.** Gaussian sampling benefits from dedicated optimized kernels, whereas PyTorch currently lacks a specialized routine for Rademacher sampling. Hence, generating Rademacher noise via `torch.randint(0, 2, size=param.data.size(), device=param.data.device, dtype=param.data.dtype) * 2 - 1` is slower than Gaussian sampling.

D Experiments on LLMs

D.1 Detailed Experiments on RoBERTa-large

We perform FZOO experiments on the RoBERTa-large model using the hyperparameters listed in Table 8. For learning rate scheduling and early stopping strategies, a constant learning rate is used in all FZOO experiments.

Table 8: The hyperparameter grids used for RoBERTa-large experiments. FZOO uses a constant learning rate schedule.

Experiment	Hyperparameters	Values
FZOO	Batch size	64
	Learning rate	$1e-4$
	μ	$1e-4$
	Weight Decay	0
FZOO (prefix)	Batch size	64
	Learning rate	$\{1e-2, 1e-1\}$
	μ	$\{1e-2, 1e-1\}$
	Weight Decay	0
	# prefix tokens	5

Table 9: Experiments on RoBERTa-large (350M parameters, k=512). For MeZO we report the results we reproduced.

Task Type	SST-2	SST-5	SNLI	MNLI	RTE	TREC	Average
	— sentiment —		— natural language inference —			— topic —	
Zero-shot	79.0	35.5	50.2	48.8	51.4	32.0	49.5
LP	91.3	51.7	80.9	71.5	73.1	89.4	76.3
FT	91.9	47.5	77.5	70.0	66.4	85.0	73.1
FT (prefix)	91.9	47.7	77.2	66.5	66.6	85.7	72.6
MeZO	93.3	53.2	83.0	78.3	78.6	94.3	80.1
MeZO (prefix)	93.3	53.6	82.9	75.6	77.2	88.2	78.4
HiZOO	95.5	53.2	82.6	77.7	80.0	94.6	80.6
HiZOO (prefix)	96.1	54.2	85.7	79.7	77.3	93.9	81.2
FZOO	94.2	55.1	84.6	79.9	79.1	95.6	81.4
FZOO (prefix)	96.1	51.5	83.1	81	76.5	95.8	80.7

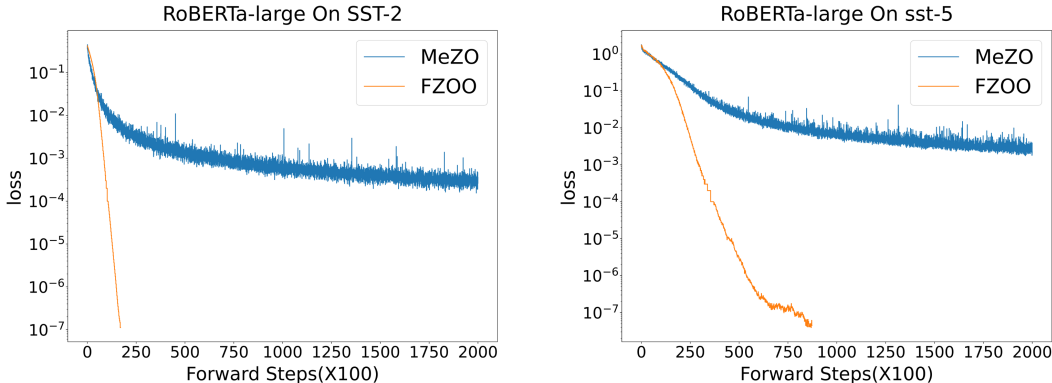


Figure 8: Loss curves on RoBERTa-large between MeZO and FZOO.

In Table 9 we show the full experiment results. Additionally, we plot more loss curves to compare with MeZO. As shown in Figure 8, we can see that FZOO can greatly accelerate the training process over MeZO, which verifies the robustness of FZOO.

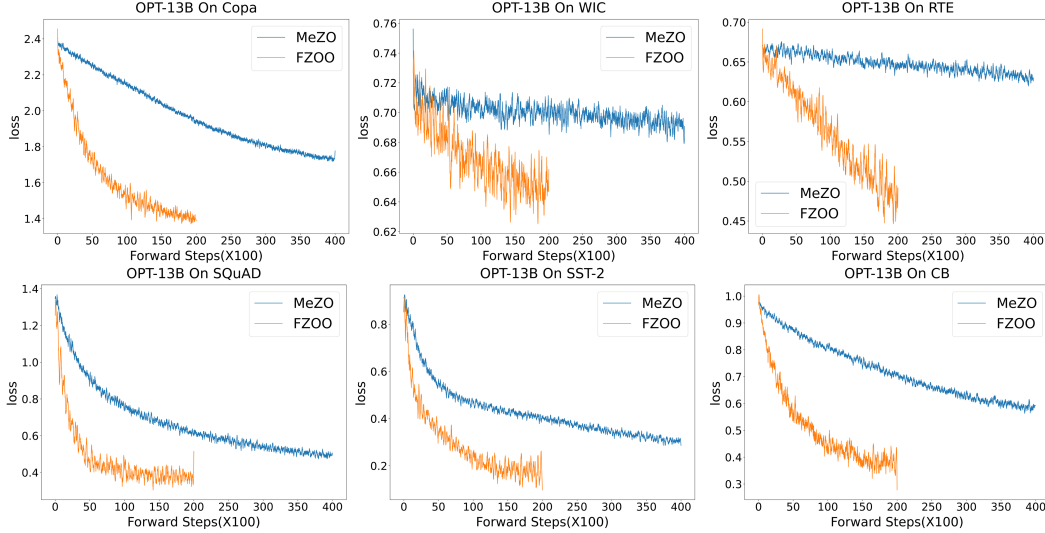


Figure 9: Loss curves on OPT.

D.2 More results on various LLMs

We use the hyperparameters in Table 10 for FZOO experiments on OPT. Full results for OPT-2.7B and OPT-125M are in Table 11. **We also provide the relative loss curves of fine-tuning OPT-13B in Figure 9.** We also provide several loss curves of fine-tuning Phi-2(2.7B) and Llama3(8B) in Figure 10 and Figure 11.

Table 10: The hyperparameter grids used for OPT experiments. All weight decay is set to 0. FZOO uses constant learning rates.

Experiment	Hyperparameters	Values
FZOO	Batch size	16
	Learning rate	$\{1e-5, 5e-5, 1e-4, 5e-4\}$
	μ	$\{1e-3, 5e-4, 1e-4\}$
FT with Adam	Batch size	8
	Learning Rates	$\{1e-5, 5e-5, 8e-5\}$

Table 11: Experiments on OPT-2.7B and OPT-125M. The best results are highlighted in bold for better comparison. We highlight the best results between FZOO and MeZO in bold to facilitate comparison.

Model	Method	SST-2	RTE	CB	BoolQ	WSC	WIC	MultiRC	COPA	ReCoRD	SQuAD	DROP	Average
OPT-2.7B	MeZO	92.2	58.8	62.5	64.0	53.8	54.2	58.4	76.0	75.0	77.6	25.3	63.4
OPT-2.7B	FZOO	93.6	69.0	62.5	70.8	57.7	57.5	65.5	83.0	76.2	81.8	26.5	67.6
OPT-125M	MeZO	81.8	55.6	67.9	60.0	60.6	54.1	58.7	64.0	52.3	44.1	14.2	55.8
OPT-125M	FZOO	84.5	60.7	67.9	61.8	60.6	57.4	61.1	64.0	50.7	51.0	15.9	57.8

E Details about Memory Usage

Here we show the detailed numbers of memory profiling results Table 12. We did not turn on any advance memory-saving options, e.g., gradient checkpointing. We set the per-device batch size as 1 to test the minimum hardware requirement to run the model with specific optimization algorithms. We use Nvidia’s `nvidia-smi` command to monitor the GPU memory usage.

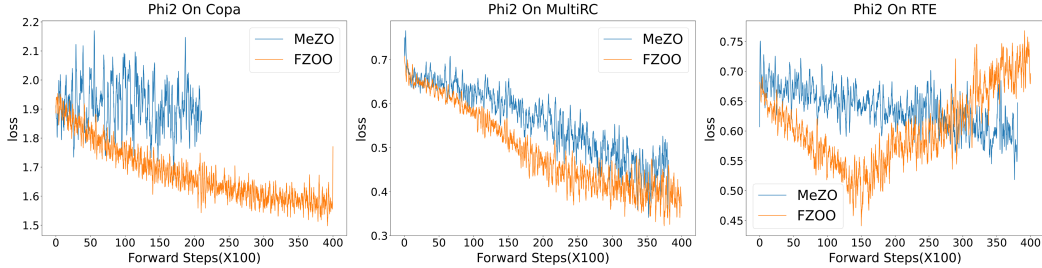


Figure 10: Loss curves on Phi-2 between MeZO and FZOO.

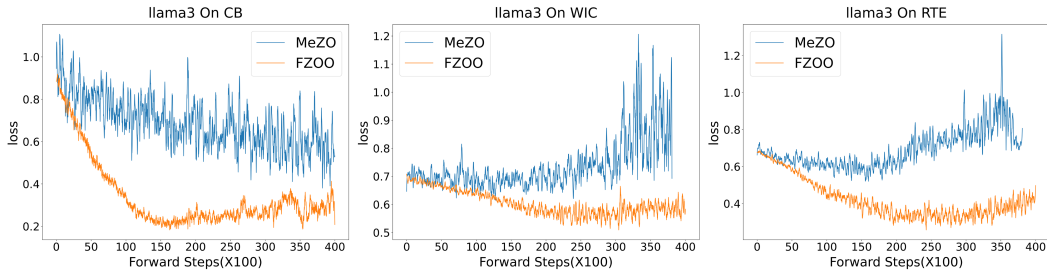


Figure 11: Loss curves on Llama3 between MeZO and FZOO.

Table 12: Memory usage on the MultiRC (average tokens=400) dataset. Results of ICL and full-parameter tuning are from MeZO[28].

Method	zero-shot/FZOO(FT)	HiZOO(FT)	Adam(Prefix)	ICL	Adam(FT)
1.3B	1xA100 (4GB)	1xA100 (7GB)	1xA100 (19GB)	1xA100 (6GB)	1xA100 (27GB)
2.7B	1xA100 (7GB)	1xA100 (13GB)	1xA100 (29GB)	1xA100 (8GB)	1xA100 (55GB)
6.7B	1xA100 (14GB)	1xA100 (29GB)	1xA100 (46GB)	1xA100 (16GB)	2xA100 (156GB)
13B	1xA100 (26GB)	1xA100 (53GB)	2xA100 (158GB)	1xA100 (29GB)	4xA100 (316GB)
30B	1xA100 (58GB)	2xA100 (118GB)	4xA100 (315GB)	1xA100 (62GB)	8xA100 (633GB)
66B	2xA100 (128GB)	3xA100 (246GB)	8xA100	2xA100 (134GB)	16xA100

F Details about Wallclock Time Efficiency

As shown in Table 13, to avoid introducing additional overheads such as inter-GPU communication, results are measured on the same dataset (RoBERTa-large use SST-2 and OPT use COPA) and GPUs (80GB A100), with each result averaged over 100 steps. "BS" refers to batch size. For the relatively smaller RoBERTa-large model, we used a BS=64, while for other models, we used a BS=16.

Table 13: Wallclock time per step between Adam, MeZO and FZOO(N=8).

Method	OPT-125M	RoBERTa-large	OPT-1.3B
Adam	0.1982s(BS=16)	0.3930s(BS=64)	0.5814s(BS=16)
MeZO	0.1368s(BS=16)	0.4305s(BS=64)	0.7218s(BS=16)
FZOO w/o parallel	0.6941s(BS=16)	1.0773s(BS=64)	3.1925s(BS=16)
FZOO	0.3835s(BS=16)	0.6052s(BS=64)	1.6628s(BS=16)

G Details about Ablation Experiments

G.1 Influence of Number of Perturbation Directions Used in Each Update

We performed an ablation study on the perturbation batch size on the SST-2 dataset using the OPT-125M model. As shown in Table 14, we observed that a batch size of 8 shows the best average performance among all tested configurations. While some other settings perform well in certain cases, batch size 8 offers a good trade-off between stability and effectiveness, suggesting that a moderate number of perturbations per step benefits the zeroth-order optimization process.

Table 14: Ablations on OPT-125M using SST-2 dataset.

Batch Size	(5e-5,1e-3)	(2e-4,5e-5)	(5e-4,1e-4)	(1e-5,1e-4)	(1e-4,1e-3)	(5e-5,5e-5)	(5e-5,1e-4)	Average
2	0.8154	0.4908	0.4908	0.4908	0.7901	0.8165	0.4908	0.6484
4	0.8360	0.7798	0.6261	0.8349	0.8211	0.8417	0.8372	0.8026
8	0.8429	0.8521	0.7626	0.8028	0.8440	0.8326	0.8417	0.8278
16	0.8326	0.8567	0.8211	0.7110	0.8440	0.8452	0.8349	0.8244
32	0.7982	0.8498	0.8429	0.5734	0.8268	0.8154	0.8119	0.7945